arXiv:1409.2817v1 [physics.flu-dyn] 9 Sep 2014

Ribbon turbulence

Antoine Venaille,[1, a)] Louis-Philippe Nadeau,[2] and Geoffrey Vallis[3]

[1)] *Laboratoire de Physique de l'École Normale Supérieure de Lyon, CNRS and Université de Lyon, 46 Allée d'Italie, 69007 Lyon, France.*

[2)] *PAOC, DEAPS, MIT, 77 Massachusetts Avenue, Cambridge, MA 02139-4307, USA.*

[3)] *CEMPS, University of Exeter, Exeter, EX4 4QF, UK.*

(Dated: 10 September 2014)

We investigate the non-linear equilibration of a two-layer quasi-geostrophic flow in a channel forced by an imposed unstable zonal mean flow, paying particular attention to the role of bottom friction. In the limit of low bottom friction, classical theory of geostrophic turbulence predicts an inverse cascade of kinetic energy in the horizontal with condensation at the domain scale and barotropization on the vertical. By contrast, in the limit of large bottom friction, the flow is dominated by ribbons of high kinetic energy in the upper layer. These ribbons correspond to meandering jets separating regions of homogenized potential vorticity. We interpret these result by taking advantage of the peculiar conservation laws satisfied by this system: the dynamics can be recast in such a way that the imposed mean flow appears as an initial source of potential vorticity levels in the upper layer. The initial baroclinic instability leads to a turbulent flow that stirs this potential vorticity field while conserving the global distribution of potential vorticity levels. Statistical mechanical theory of the 1-1/2 layer quasi-geostrophic model predict the formation of two regions of homogenized potential vorticity separated by a minimal interface. We show that the dynamics of the ribbons results from a competition between a tendency to reach this equilibrium state, and baroclinic instability that induces meanders of the interface. These meanders intermittently break and induce potential vorticity mixing, but the interface remains sharp throughout the flow evolution. We show that for some parameter regimes, the ribbons act as a mixing barrier which prevent relaxation toward equilibrium, favouring the emergence of multiple zonal jets.

[a)]Electronic mail: antoine.venaille@ens-lyon.fr

I. INTRODUCTION

A striking property of observed oceanic mesoscale turbulence (from 10 to 1000 km) is the ubiquity of jets with a typical width of order the internal Rossby radius of deformation, R. In quasi-geostrophic theory $R = NH/f$ where N is the buoyancy frequency, H is a vertical scale and f is the Coriolis parameter, and in the ocean $R \sim 50$ km. These jets are robust coherent structures but with high variability characterized by strong meanders — as, for example the case of the Gulf-Stream or the Kuroshio. Sometimes these meanders break into an isolated vortex, in which case the jets are curled into rings that literally fill the oceans. What set the strength, the horizontal size and the vertical structure of mesoscale eddies is a longstanding problem in physical oceanography. Here we address this question in a two-layer quasi-geostrophic model, with a particular focus on the role of bottom friction. We consider the equilibration of an initial perturbation in a channel with an imposed constant vertical shear U in the zonal (eastward) direction. This model might be considered as one of the elementary building blocks of a hierarchy of more complex models that describe oceanic or atmospheric turbulence[1,2]. One motivation for this model is that the main source of energy for these turbulent flows comes from baroclinic instability that releases part of the huge potential energy reservoir set at large scale by wind forcing at the surface of the oceans or solar heating in the atmosphere[3].

Bottom friction is the main sink of kinetic energy and without it there will be no nonlinear equilibration, so it is important to fully understand its role. A crude but effective model of that bottom friction, based on Ekman-layer dynamics, is simply linear drag with coefficient r. Given this, the two-layer model has two important nondimensional parameters: the ratio R/L_y, with L_y the width of the channel, and the ratio rR/U which is a measure of the bottom friction time scale to an inertial time scale based on the Rossby radius of deformation. There are other important parameters if the Coriolis parameter is allowed to vary but these are not our particular concern here.

In the low bottom friction limit, classical arguments based on cascade phenomenology predict an inverse cascade of kinetic energy in the horizontal with a concomitant tendency toward barotropization on the vertical, i.e. the emergence of a depth independent flow[4–6]. In a closed finite-sized domain, the inverse energy cascade on the horizontal leads to condensation of the eddies at the domain scale. The intermediate regime ($rR/U \sim 1$) has been

studied by Thompson and Young[7], using vortex gas kinetics since the flow is made in that case of a multitude of isolated vortices or dipoles. The high bottom friction limit has been studied numerically by Arbic and Flierl[8 9], who also proposed scaling arguments for the vertical structure of the flow. They observed the spontaneous formation of coherent jets in the upper layer. The typical width of these jets was given by the Rossby radius of deformation of the upper layer. Arbic and Flierl[8] noticed that these coherent jets looked like localized, thin and elongated ribbons of high kinetic energy regions. These ribbons were reported to interact together in a seemingly erratic way through meandering, pinching, coalescence and splitting of the regions separating them. Accordingly, the high bottom friction regime will be referred to in the following as "ribbon turbulence".

The numerical results of Thompson and Young[7], Arbic and Flierl[9] were all performed in a doubly periodic domain and one novelty of our work is to consider a channel geometry. A particular advantage of the the channel geometry is that, with a proper re-definition of the potential vorticity, the dynamics in the upper layer can be recast in the form of an advection equation for the potential vorticity field, without sources or sinks, whereas in a doubly-periodic the beta term associated with the imposed mean flow must be subtracted off in order to avoid a potential vorticity discontinuity at the boundary. We will discuss the physical consequences of these conservations laws in the low bottom friction limit and in the high bottom friction limit. This will allow us to revisit the barotropization process in the weak bottom friction limit, and the emergence of ribbons in the high bottom friction limit. In particular, we will interpret the emergence of ribbons as a tendency to reach a statistical equilibrium state. Statistical mechanical theory provides predictions for the self-organization properties of two-dimensional and quasi-geostrophic flows, and was initially proposed by Miller[10], Robert and Sommeria[11]. The theory applies to freely evolving flow (without forcing and dissipation), and explains self-organization of the flow into the most probable state as the outcome of turbulent stirring, and allows to compute this most probable state. In practice, the computation of the statistical equilibria requires the knowledge of a few key parameters as the energy and the global potential vorticity distribution as an input.

When bottom friction is large, the two-layer quasi-geostrophic dynamics is strongly dissipated, and one might expect that any prediction of the equilibrium theory applied to this two-layer flow would fail. However, we will argue that key features of the equilibrated states, including the emergence of ribbons, can be accounted for by considering equilibrium states

of a 1-1/2 layer quasi-geostrophic turbulence, which amounts to assume that only the upper layer is "active". It has been shown previously that when the Rossby radius is small, equilibrium states of the 1-1/2 layer quasi-geostrophic model contain two regions of homogenized potential vorticity, with a thin interface between these regions[12]. We will explain why this is relevant to describe the emergence of ribbons and provide a complementary point of view based on cascade arguments. We will go further than the application of equilibrium statistical mechanics in order to account for some of the dynamical aspects of the ribbons. In particular, we will show that the observed meanders of the ribbons cannot be explained in the framework of 1-1/2 layer quasi-geostrophic model, but must be accounted for by the baroclinic instability of the ribbons in the framework of a two-layer quasi-geostrophic model. We will also see that once a ribbon is formed, it may act as a mixing barrier and prevent relaxation towards the equilibrium state. For this reason, more than two regions of homogenized regions can coexist for some range of parameters. We will relate this observation to the emergence of multiple zonal jets in this flow model.

The paper is organized as follows. The basic model is presented in section II along with a discussion of the physical consequences of existing conservation laws for the dynamics. In section III we review existing results based on cascade arguments and statistical mechanics approach and give predictions for the flow structure at large times. These predictions are tested against numerical simulations in a section IV, and we conclude in section V.

II. BAROCLINIC TURBULENCE IN A TWO-LAYER QUASI-GEOSTROPHIC FLOW

A. Two layer quasi-geostrophic flows in a channel

We consider a two-layer quasi-geostrophic model on a f-plane in a channel periodic in the x direction and of size $(L_x \times L_y)$ (Fig 1-a). The relative depth of the upper and lower layers are $\delta = H_1/H$ and $1-\delta = H_2/H$, respectively, with H the total depth. Consequently, the internal Rossby radius of deformation of the upper and the lower layer are $R_1 = \delta^{1/2} R$ and $R_2 = (1-\delta)^{1/2} R$, respectively, with $R = (Hg')^{1/2}/f_0$, with g' the reduce gravity between the two layers, and f_0 the Coriolis parameter. The dynamics is given by the advection in each layer of the potential vorticity fields q_1, q_2 by a non-divergent velocity field which can

be expressed in term of a streamfunction Ψ_1, Ψ_2 :

$$\partial_t q_1 + J(\Psi_1, q_1) = -A_h \nabla^6 \Psi_1, \tag{1}$$

$$\partial_t q_2 + J(\Psi_2, q_2) = -A_h \nabla^6 \Psi_2 - r\nabla^2 \Psi_2 \ , \tag{2}$$

where A_h is a lateral bi-harmonic viscosity coefficient, r is a bottom drag coefficient, $J(a,b) = \partial_x a \partial_y b - \partial_y a \partial_x b$ is the Jacobian operator. The velocity field in each layer is given by $U_i = -\partial_y \Psi_i$, $V_i = \partial_x \Psi_i$, for $i = 1, 2$. The potential vorticity fields are expressed as the sum of a relative vorticity term $\zeta_i = \nabla^2 \Psi_i$ and a stretching term involving the Rossby radius of deformation R:

$$q_1 = \nabla^2 \Psi_1 + \frac{\Psi_2 - \Psi_1}{\delta R^2}, \tag{3}$$

$$q_2 = \nabla^2 \Psi_2 + \frac{\Psi_1 - \Psi_2}{(1-\delta) R^2} \ . \tag{4}$$

These equations must be supplemented with boundary conditions. The flow is periodic in the x direction, and there is no flow across the wall at the northern and the southern boundaries. This impermeability constraints amounts to assume that $\Psi_{1,2}$ is a constant at the northern and the southern boundary. Four equations are then needed to determine these constants. Two equations are given by mass conservation, which imposes the constraints

$$\int_{\mathcal{D}} \mathrm{d}x\mathrm{d}y \Psi_1 = \int \mathrm{d}x\mathrm{d}y \Psi_2 = 0 \ . \tag{5}$$

Two additional equations are obtained by integrating over one line of constant latitude (constant y) the zonal projection (along $\mathbf{e}_x$) of the momentum equations in each layers. Let us consider the particular case where the line of constant latitude is the southern boundary, and let us call $\Gamma_i = \int_0^{L_x} \mathrm{d}x U_i(x,0)$ the circulation along this boundary. Then the two additional equations are

$$\frac{d\Gamma_1}{dt} = -A_h \left(\int_0^{L_x} \mathrm{d}x \nabla^4 U_1 \Big|_{y=0} \right), \quad \frac{d\Gamma_2}{dt} = -A_h \left(\int_0^{L_x} \mathrm{d}x \nabla^4 U_2 \Big|_{y=0} \right) - r\Gamma_2, \tag{6}$$

see Pedlosky [13] for further details on the quasi-gesotrophic dynamics in an open channel.

In the absence of small scale dissipation (i.e. when $A_h = 0$), the dynamics is fully determined by Eq. (1-2-6-5). When small scale dissipation is taken into account (i.e. when $A_h \neq 0$), additional boundary conditions are required due to higher order terms appearing in Eq. (1-2-6) . We will consider in numerical simulations a free-slip boundary condition: the vorticity is set to zero at the southern and northern boundary of each layer.

B. Evolution of a perturbation around an imposed mean flow

We impose the existence of a constant eastward flow in the upper layer with a lower layer at rest ($\overline{\Psi}_1 = -Uy$, $\overline{\Psi}_2 = 0$). We denote ψ_1 and ψ_2 the perturbation around this mean flow ($\psi_i = \Psi_i - \overline{\Psi}_i$). The potential vorticity fields defined Eq. (3-4) can be written in term of this perturbed streamfunction :

$$q_1 = \nabla^2\psi_1 + \frac{\psi_2 - \psi_1}{\delta R^2} + \frac{U}{\delta R^2} y \ , \tag{7}$$

$$q_2 = \nabla^2\psi_2 + \frac{\psi_1 - \psi_2}{(1-\delta)\, R^2} - \frac{U}{(1-\delta)\, R^2} y \ . \tag{8}$$

We see that the mean flow is associated with a zonal potential vorticity gradient (an "effective beta plane" term) having an opposite sign in the upper and lower layer. The dynamics of the perturbation is then fully described by the potential vorticity advection:

$$\partial_t q_1 + J\left(\psi_1 - Uy, q_1\right) = -A_h \nabla^6 \psi_1 \ , \tag{9}$$

$$\partial_t q_2 + J\left(\psi_2, q_2\right) - A_h \nabla^6 \psi_2 - r\nabla^2\psi_2 \ . \tag{10}$$

When this equation is linearized around the mean flow, we recover the Philipps model for baroclinic instability on a f-plane, see e.g. Vallis[3]. In this configuration, the mean flow is always unstable and the most unstable mode is always associated with an horizontal scale that scales with the internal Rossby radius of deformation, whatever the value of bottom friction. Only the time scale for the instability changes with bottom friction. Our aim is to study the non-linear equilibration of this instability.

C. Conserved quantities

The flow model has a remarkable property: in the absence of small scale dissipation, the potential vorticity in the upper layer q_1 is advected without sinks nor sources. As a consequence, there is an infinite number of conserved quantities, namely the Casimir functionals $\mathcal{C}_s[q_1] = \int_D \mathrm{d}x\mathrm{d}y \ s(q_1)$, where s is any sufficiently smooth function, see also Shepherd[14]. An equivalent statement is that the global distribution of the potential vorticity levels in the upper layer is conserved through the flow evolution when there is no small scale dissipation. Since the initial flow is characterized by $q_1\big|_{t=0} = Uy/(\delta R^2)$, the global distribution of fine grained potential vorticity in the upper layer is a flat distribution of

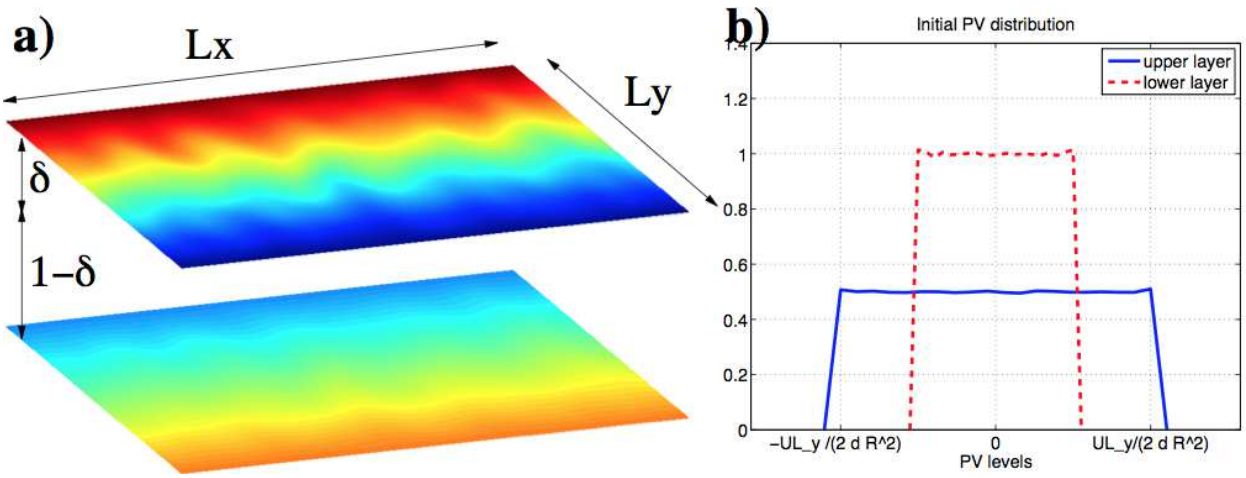

FIG. 1. Sketch of the numerical experiment. Left panel: potential vorticity field at the beginning of the simulation, when the most unstable mode start to grow, in the case without bottom friction. Right panel global distribution of potential vorticity levels at t=0, which is the same whatever the bottom friction. .

potential vorticity levels between $-UL_y/(2\delta R^2)$ and $UL_y/(2\delta R^2)$, see Fig. 1-b. Similarly, the global distribution of the potential vorticity in the lower layer is conserved if both the small scale dissipation and the bottom friction are zero. In that case, given our initial potential vorticity profile, the global distribution of potential vorticity levels in the lower layer is a flat distribution between $-UL_y/(2\delta R^2)$ and $UL_y/(2(1-\delta)R^2)$, see Fig. 1. If bottom friction is non zero, the potential vorticity distribution of the lower layer is not conserved, but the potential vorticity distribution of the lower layer remains bounded. Remarkably, the presence of bottom friction does not affect conservation of the potential vorticity distribution in the upper layer.

When there is small scale dissipation, the global distribution of potential vorticity levels is no more a conserved quantity. However, if the time scale for the relaxation of the initial condition towards a quasi-stationary state is smaller than the typical dissipation time scale, then one expects that the conservation laws of the inviscid dynamics still plays an important role.

D. Energy budget

The energy of the perturbation is the sum of kinetic energy in each layer and of the available potential energy:

$$E = KE_1 + KE_2 + APE, \quad APE = \frac{1}{2}\int_{\mathcal{D}} \mathrm{d}x\mathrm{d}y \, \frac{(\psi_1 - \psi_2)^2}{R^2}, \tag{11}$$

$$KE_1 = \frac{\delta}{2}\int_{\mathcal{D}} \mathrm{d}x\mathrm{d}y \, (\nabla\psi_1)^2, \quad KE_2 = \frac{1-\delta}{2}\int_{\mathcal{D}} \mathrm{d}x\mathrm{d}y \, \ (\nabla\psi_2)^2 \, . \tag{12}$$

In the absence of small scale dissipation, the temporal evolution of the energy of the perturbation is given by

$$\frac{R}{U}\frac{\mathrm{d}}{\mathrm{d}t}E = \frac{1}{R}\int_{\mathcal{D}} \mathrm{d}x\mathrm{d}y \, \psi_1\partial_x\psi_2 - (1-\delta)\frac{rR}{U}\int_{\mathcal{D}} \mathrm{d}x\mathrm{d}y \, \ (\nabla\psi_2)^2 \ . \tag{13}$$

We readily note that the parameter rR/U plays a key role in the energy budget (13), and that this energy budget for the perturbed flow is the same as one would obtain in the doubly periodic geometry[9]. In the channel geometry, it is also useful to introduce the "total energy" defined as the energy of the flow that includes the perturbation and the mean flow:

$$E_{tot} = KE_{1tot} + KE_{2tot} + APE_{tot}, \quad APE_{tot} = \frac{1}{2}\int_{\mathcal{D}} \mathrm{d}x\mathrm{d}y \, \frac{(\psi_1 - Uy - \psi_2)^2}{R^2}, \tag{14}$$

$$KE_{1tot} = \frac{\delta}{2}\int_{\mathcal{D}} \mathrm{d}x\mathrm{d}y \, (\nabla\psi_1 - Uy)^2, \quad KE_{1tot} = \frac{1-\delta}{2}\int_{\mathcal{D}} \mathrm{d}x\mathrm{d}y \, (\nabla\psi_2)^2. \tag{15}$$

The temporal evolution of the total energy is given by

$$\frac{\mathrm{d}}{\mathrm{d}t}E_{tot} = -(1-\delta)r\int_{\mathcal{D}} \mathrm{d}x\mathrm{d}y \, \ (\nabla\psi_2)^2 \ . \tag{16}$$

This equations for the total energy allows for a clear physical interpretation in the channel case: in the presence of bottom friction, the total energy will decay to zero. In other words, the perturbation will evolves toward the state $\psi_1 = -Uy$, $\psi_2 = 0$ which annihilates the imposed mean flow. We see from Eq. (7-8) that such a state corresponds to fully homogenized potential vorticity fields $q_1 = q_2 = 0$. Note that this potential vorticity homogenization process does not rely on the existence of small scale dissipation, since the potential vorticity can be homogenized at a coarse grained level. The important mechanism is the filamentation process following sequences of stretching and folding of the potential vorticity field through turbulent stirring.

We will see in the following that the route towards complete potential vorticity homogenization strongly depends on the parameter rR/U. In particular, dimensional analysis predicts that the time scale for homogenization can be written on the general form

$$t_{diss} \sim \frac{1}{r} F_{diss}\left(\frac{rR}{U}, \frac{R}{L_y}, \delta, \frac{L_x}{L_y}\right), \tag{17}$$

where the argument of the function F_{diss} are the four non-dimensional parameters of the problem, assuming vanishing small scale dissipation ($A_h = 0$). We will argue in the next section that when the domain is large with respect to the Rossby radius of deformation ($L_y \gg R$), when the upper layer is thin with respect to the total depth ($\delta \ll 1$) and when the domain aspect ration is of order one ($L_x \sim L_y$) the function F_{diss} can be modeled by xx check if $\delta \ll 1$ is necessary xx.

$$F_{diss} = 1 + \frac{1-\delta}{\delta^{1/2}} \left(\frac{rR}{U}\right)^2 \frac{L_y}{R}. \tag{18}$$

For that purpose, we will need to discuss the vertical and the horizontal flow structure at large time, before complete homogenization is achieved.

III. PREDICTIONS FOR THE FLOW STRUCTURE AT LARGE TIME

The aim of this section is to provide predictions for the vertical partition of the energy, and to explore consequences of this vertical structure for the self-organization of the flow on the horizontal. We first show that barotropization is expected for vanishing bottom friction. We then explain that surface intensification is expected for large bottom friction. We then use a combination of arguments based on cascade phenomenology, potential vorticity homogenization theories and equilibrium statistical mechanics in order to predict the horizontal flow structure in the large bottom friction limit and the small bottom friction limit. It is assumed in this section that the small scale dissipation is negligible ($A_h = 0$).

A. Barotropization in the low bottom friction limit

We consider first the case with zero bottom friction ($r = 0$). It will be useful to consider the barotropic and baroclinic modes of the two-layer model, defined as

$$\psi_t = \delta\psi_1 + (1-\delta)\,\psi_2, \quad \psi_c = \psi_1 - \psi_2\ . \tag{19}$$

The baroclinic streamfunction ψ_c and the barotropic streamfunction ψ_t are related to the potential vorticity through

$$q_1 - q_2 = \nabla^2 \psi_c - \frac{\psi_c}{\delta(1-\delta)R^2} - \frac{U}{\delta(1-\delta)R^2} y \tag{20}$$

$$\delta q_1 + (1-\delta) q_2 = \nabla^2 \psi_t \tag{21}$$

The energy of the perturbation can be decomposed into a (purely kinetic) barotropic energy and a baroclinic energy that involves both kinetic energy and potential energy:

$$E = KE_t + KE_c + APE_c, \quad APE_c = \frac{1}{2} \int_{\mathcal{D}} \mathrm{d}x\mathrm{d}y \, \frac{\psi_c^2}{R^2}. \tag{22}$$

$$KE_t = \frac{1}{2} \int_{\mathcal{D}} \mathrm{d}x\mathrm{d}y \, \left(\nabla \psi_t\right)^2, \quad KE_c = \delta\,(1-\delta)\,\frac{1}{2} \int_{\mathcal{D}} \mathrm{d}x\mathrm{d}y \, \left(\nabla \psi_c\right)^2. \tag{23}$$

Similarly, the total energy can be decomposed into a barotropic and a baroclininc component:

$$E = KE_{tot,t} + KE_{tot,c} + APE_{tot,c}, \quad APE_{tot,c} = \frac{1}{2} \int_{\mathcal{D}} \mathrm{d}x\mathrm{d}y \, \frac{\left(\psi_c - Uy\right)^2}{R^2}. \tag{24}$$

$$KE_{tot,t} = \frac{1}{2} \int_{\mathcal{D}} \mathrm{d}x\mathrm{d}y \, \left(\nabla(\psi_t - \delta U y)\right)^2, \quad KE_{tot,c} = \delta\,(1-\delta)\,\frac{1}{2} \int_{\mathcal{D}} \mathrm{d}x\mathrm{d}y \, \left(\nabla\left(\psi_c - U y\right)\right)^2. \tag{25}$$

The initial potential vorticity fields in the upper and lower layers are respectively $q_1^0 = Uy/\delta R^2$ and $q_2^0 = -Uy/(1-\delta)R^2$, plus a small perturbation. When $R \ll L_y$ or $\delta \ll 1$, and when $L_x \sim L_y$, the initial total energy is dominated by the potential energy: $E_{tot}^0 \sim APE_{tot}^0 \sim U^2 L_y^4 / R^2$.

The classical picture for two layer geostrophic turbulence predicts that the turbulent evolution of the flow leads to barotropization[4–6], i.e. to a depth independent flow for which $E_{tot} \approx KE_{tot,t}$. In the context of freely evolving inviscid dynamics, the idea that barotropization may occur as a tendency to reach a statistical equilibrium state that takes into account dynamical invariants has been investigated by Refs.[15–17]. It was found in these studies that barotropization may be prevented by conservation of potential vorticity levels in some cases. We provide in Appendix A a phenomenological argument for barotropization in the case $R \ll L_y$ or $\delta \ll 1$, emphasizing the role of the conservation of potential vorticity levels, and of the total energy. In this limit, the flow dynamics is described at lowest order by the barotropic dynamics after its initial turbulent rearrangement:

$$\partial_t q_t + J(\psi_t, q_t) = 0, \quad q_t = \nabla^2 \psi_t. \tag{26}$$

Let us now discuss the effect of a weak friction $rR/U \ll 1$. Let us call $t_{adv} = L_y/U$ the typical advection time scale for the flow over the whole domain. This can be considered as the typical time scale for the self-organization of the turbulent dynamics following the initial instability that occurs on a time scale $t_{inst} = R/U$. Once the flow is self-organized at the domain scale, if the flow is dominated by the barotropic mode, we see Eq. (16) that the total energy should decay exponentially with an e-folding time $t_{fric} \sim 1/(1-\delta)r$. This justifies the low friction limit for the function F_{diss} defined Eq. (18).

B. Surface intensification in the large bottom friction limit

In the large bottom friction limit, if the system reaches or a quasi-stationary state, we see from the energy budget Eq. (13) for the perturbed flow that the friction term $(1-\delta)(rR/U)\int_{\mathcal{D}} \mathrm{d}x\mathrm{d}y \ (\nabla\psi_2)^2$ must be of the order of the source term $(1/R)\int_{\mathcal{D}} \mathrm{d}x\mathrm{d}y \ \psi_1\partial_x\psi_2$. Anticipating that typical horizontal scales of the flow structures will be given by $\delta^{1/2}R$, we find that typical variations of the stream function in the lower and the upper layers are related through

$$\psi_1 \sim (1-\delta)\,\frac{rR}{U}\psi_2. \tag{27}$$

We conclude that $\psi_1 \gg \psi_2$ when $rR/U \gg 1$. At lowest order, only the upper layer is active and the flow can be described by a 1-1/2 layer quasi-geostrophic model:

$$\partial_t q_1 + J\left(\Psi_1, q_1\right) = 0 \ , \tag{28}$$

with the notation $\Psi_1 = \psi_1 - Uy$ and with

$$q_1 = \nabla^2\Psi_1 - \frac{\Psi_1}{\delta R^2}. \tag{29}$$

Let us now estimate the typical time scale for the energy evolution. Anticipating the emergence of ribbons, we assume that the total energy is dominated by the potential energy $E_{tot} \sim L_y^2\Psi_1^2/R^2$. This energy should decay with time according to Eq. (16). We use the scaling Eq. (27) to estimate $\int_{\mathcal{D}} \mathrm{d}x\mathrm{d}y\,(\nabla\psi_2)^2 \sim U^2\psi_1^2 L_y/(r^2\delta^{1/2}(1-\delta)^2R^3)$. Introducing the dissipation time t_{diss} such that $dE_{tot}/dt \sim E_{tot}/t_{diss}$, and assuming $\psi_1 \sim \Psi_1$ we get

$$t_{diss} \sim \frac{1}{r}\frac{1-\delta}{\delta^{1/2}}\left(\frac{rR}{U}\right)^2\frac{L_y}{R} \tag{30}$$

This leads to a surprising result: in the large bottom friction limit, the typical time scale for the evolution of the quasi-stationary large scale flow is proportional to the bottom friction coefficient. This estimate for the dissipation time Eq. (30) justify our choice for F_{diss} Eq. (18) in the limit $rR/U \gg 1$ and $\delta^{1/2}R \ll L_y$. The main caveat of this argument is to assume $\psi_1 \sim \Psi_1$ which can not be valid at short time (when the instability grows) and at large time (when the perturbation has almost annihilated the mean flow). However, we will show that this provides a reasonable scaling to interpret the numerical simulations. In addition, same argument applied to the energy budget of the perturbed flow Eq. (16), without assuming $\psi_1 \sim \Psi_1$, would show that t_{diss} is the typical time scale for the growth of the potential energy of the perturbed state.

C. Cascade phenomenology for quasi-geostrophic models

The flow in the large friction limit $rR/U \gg 1$ and in the low friction limit $rR/U \ll 1$ are both described at lowest order by a one layer flow model:

$$\partial_t q + J(\psi, q) = 0, \quad q = \nabla^2\psi - \lambda_d^{-2}\psi \ . \tag{31}$$

We recover the barotropic dynamics Eq. (26) when $\lambda_d = +\infty$ and the 1-1/2 layer quasi-geostrophic dynamics Eq. (28-29) when $\lambda_d = \delta^{1/2}R$.

We consider Eq. (31) with an arbitrary λ_d and we introduce the relative vorticity $\zeta = \nabla^2\psi$. At spatial scales much smaller than λ_d the potential vorticity q is dominated by the relative vorticity and the dynamics is given by 2d Euler equations:

$$\partial_t \zeta + J(\psi, \zeta) = 0. \tag{32}$$

Classical arguments[18,19] predict a direct cascade of enstrophy $Z = \int_{\mathcal{D}} \mathrm{d}x\mathrm{d}y \ \zeta^2/2$ and an inverse cascade of kinetic energy $KE = -\int_{\mathcal{D}} \mathrm{d}x\mathrm{d}y \ \psi\zeta/2$. In the freely evolving case, one expects a decrease of the energy k-centroids $k_E = \int \mathrm{d}k \ k\mathcal{E}(k)/E$ until the energy is condensed at the domain scale, and a concomitant increase of the enstrophy k-centroids $k_Z = \int \mathrm{d}k \ k\mathcal{Z}(k)/E$, where $\mathcal{E}(k)$ and $\mathcal{Z}(k)$ are the energy and enstrophy spectra[20].
At spatial scales much larger than λ_d, the dynamics Eq. (31) is the so-called planetary geostrophic model[21]:

$$\partial_\tau \psi + J(\zeta, \psi) = 0, \tag{33}$$

with $\tau = \delta R^2 t$. The role of ζ and ψ are switched with respect to the Euler dynamics. Same arguments than in the Euler case predict a direct cascade of kinetic energy KE, and an inverse cascade of potential energy[22,23] $APE = \int_{\mathcal{D}} \mathrm{d}x\mathrm{d}y\ \psi^2)/(2\lambda_d^2)$. In the freely evolving case, one expects that the available potential energy centroids will go to large scale until condensation at the domain scale. Meanwhile, the kinetic energy centroids should go to small scales.

We see that both the small scale limit described by Eq. (32) and in the large scale limit described Eq. (33), the kinetic energy is expected to pile up at scale $\lambda_d = \delta^{1/2} R$.

We also note that the concomitant condensation of potential energy at the domain scale with a direct cascade of kinetic energy (halted around the scale $\delta^{1/2} R$) is necessarily associated with the formation of large regions of homogenized streamfunction at a coarse grained level (or equivalently homogenized potential vorticity). In other words, the streamfunction gradients are expelled at the boundary between regions of homogenized potential vorticity. This justifies with a dynamical point of view the emergence of ribbons. Another complementary point of view is to say that the dynamics tends to homogenize the potential vorticity field, but that a complete homogenization would not be possible due to energy conservation. In the limit $\delta^{1/2} R \ll L_y$, the dynamics will therefore tend to form at least two regions of homogenized potential vorticity at the domain scale, which allows to sustain a large scale available potential vorticity field, while allowing for potential vorticity homogenization almost everywhere.

Typical values of the potential vorticity in the region where it is homogenized can be estimated as $\mathcal{Q}_1 \sim UL/\delta R^2$. We see from Eq. (31) that sufficiently far from the interface, between two regions of homogenized potential vorticity the streamfunction is also a constant with $\Psi_1 \sim \delta R^2 R^2 \mathcal{Q}_1 \sim U L_y$. The interfaces between different regions of homogenized potential vorticity correspond therefore to jumps of the streamfunction, which occurs at a typical scale R. This corresponds to strong an localized jets with velocity $V \sim \Psi_1/R \sim UL/R$. The length of these jets is of order of the domain size L_y, much larger than their width, of order $\delta^{1/2} R$, hence the term "ribbons".

To conclude, the flow should self-organize into a large scale structure with velocity variations at the scale of the domain L_y in the low bottom friction limit $rR/U \ll 1$, and form ribbons of width $\delta^{1/2} R$ and length L_y in the large bottom friction limit $rR/U \gg 1$. More detailed predictions for this large scale flow structure can be obtained in the framework of

equilibrium statistical mechanics, as discussed in the following subsection.

D. Statistical mechanics predictions for the large scale flow structure

Turbulent dynamics stretches and folds potential vorticity filaments which thus cascade towards smaller and smaller scales. This stirring tends to mix the potential vorticity field at a coarse-grained level, even in the absence of small scale dissipation. If there is no energy constraint and if there is enough stirring, the potential vorticity field should be fully homogenized just as in the case of a passive tracer. By contrast, complete homogenization can not be achieved if there is an energy constraint, which leads to non trivial large scale flow structures, and statistical mechanics gives a prediction for such large scale flows. The aim of this subsection is to review existing results on the statistical mechanics theory for one layer quasi-geostrophic models that will be useful to interpret our numerical results.

1. Miller-Robert-Sommeria (MRS) theory for a barotropic model

The theory was initially developed by Robert and Sommeria[11], Miller, Weichman, and Cross[24], and will be referred to as the MRS theory in the following. We provide here a short and informal presentation of this approach — see also reviews by Refs.[25–28].

The theory provides a variational problem that allows to compute the most probable outcome of turbulent stirring at a macroscopic (or coarse-grained) level among all the microscopic configurations of the flow that satisfy the constraints of the dynamics given by the conservation of the energy and of the global distribution of potential vorticity levels. Large deviation theory allows then to show that an overwhelming number of microscopic states corresponds to the most probable macroscopic state. The only assumption is ergodicity, i.e. that there is sufficient mixing in phase space for the system to explore all the possible configurations given the dynamics constraints.

In the case of a one layer quasi-geostrophic flow described by Eq. (31), the input of the theory is given by the energy of the flow E and the initial fine-grained (or microscopic) potential vorticity distribution $\gamma(\sigma)$. The output of the theory is a field $p(x, y, \sigma)$ that gives the probability density function to measure a potential vorticity level $\sigma \in \Sigma$ in the vicinity of the point (x, y). This field defines a macroscopic state of the system, which allows to

keep track of the dynamical constraints. The computation of the equilibrium state amounts to find the field p that maximizes a mixing entropy $\mathcal{S} = -\int_\Sigma \mathrm{d}\sigma \int_\mathcal{D} \mathrm{d}x\mathrm{d}y\ p\ln p$ with the constraints given by dynamical invariants expressed in term of p. This entropy counts the number of micro states associates with a given macro state p[11,24]. The constraints are given by the conservation of the global distribution $\gamma(\sigma) = d_\sigma$ with $d_\sigma[p] = \int_\mathcal{D} \mathrm{d}x\mathrm{d}y \int \mathrm{d}\sigma p$, and the energy conservation $E = \mathcal{E}[p]$ with $\mathcal{E}[p] = -\int_\mathcal{D} \mathrm{d}x\mathrm{d}y \int \mathrm{d}\sigma\sigma p\psi$. Note that the energy constraint is obtained by assuming that the energy of local vorticity fluctuations is negligible. The validity of this mean-field treatment can be proven using large deviation theory. The potential vorticity field of the equilibrium state is $\overline{q} = \int_\Sigma \mathrm{d}\sigma\ \sigma p$, and the streamfunction is obtained by inverting $\overline{q} = \nabla^2\psi - \lambda_d^{-2}\psi$. We stress that the theory applies for flows without small scale dissipation. In the presence of small scale dissipation, the predictions of the theory is expected to be valid only if the typical time scale for self organization of the flow is much smaller than the typical time associated with small scale dissipation. We also note that in that case, once the flow is self-organized, small scale dissipation smears out local fluctuations of the potential vorticity field so that the microscopic potential vorticity field q actually tends to the macroscopic field $\overline{q}$.

The equilibrium state is always characterized by a monotonous functional relation $\overline{q} = g(\psi)$[11,24]. This function g depends only on the dynamical invariants. At this stage two approaches could be followed. A first approach is to consider E and $g(\sigma)$ as given, to compute the function g, and the flow structure associated with the corresponding equilibrium state. A second approach is to assume a given $q - \psi$ relation, and to compute the MRS statistical equilibria associated with this relation. This second approach has made possible several analytical results in the last decade, and we will rely on these results to interpret our simulations.

Although computation of the equilibrium state is a difficult task in general, several analytical results can be obtained in limit cases[27] for a detailed discussion. For instance, whatever the initial distribution of potential vorticity levels, it can be shown that low energy state are always characterized at lowest order by a linear $q - \psi$ relationship, whose coefficient only depend on the total energy, the total enstrophy and the circulation[27]. Here low energy means that the energy of the flow is much smaller than the maximum admissible energy for a given potential vorticity distribution. In our case the initial total energy is of the order of $U^2L_y^3L_x/R^2$. It is not difficult to construct a state, with the same global distribution of

potential vorticity levels, that is characterized by an energy that scales as $U^2 L_y^3 L_x/(\delta R^4)$, which is therefore much larger than the initial energy provided that $\delta R \ll L_y$This justifies the low energy limit for the weak friction case.

Such a low energy limit allows us to compute analytically phase diagrams for the flow structure and to describe how this flow structure changes when the energy or the enstrophy of the flow are varied. For instance statistical equilibria associated with a linear $q - \psi$ relation have been classified for various flow model in an arbitrary close domain[29,30] and on a channel[31]. In particular, it was shown in these studies that when the flow domain is sufficiently stretched in the x direction, then the equilibrium state is a dipolar flow.

2. Application to the 1-1/2 layer quasi-geostrophic model

In the large friction limit $rR/U \gg 1$, our justification for the relevance of the "low energy limit" of the previous subsection is no more valid, since this justification relied on the estimate Eq. (35) with the underlying assumption that the flow is fully barotropic. We have shown previously that in the large friction limit, the flow is not barotorpic, but is described at lowest order by the 1-1/2 quasi-geostrophic dynamics Eq. (31) with $\lambda_d = \delta^{1/2} R$. When $\delta^{1/2} R \ll L_y$, i.e. when the Rossby radius of the upper layer is much smaller than the domain scale, it has been shown by Bouchet and Sommeria [12] that a class of equilibrium state different that the low energy states of the previous section can be computed analytically. Assuming that the $q - \psi$ relation is tanh-like, they showed that the equilibrium state is composed of two subdomains with homogenized potential vorticity separated by jets of width $\delta^{1/2} R$ at their interface, see also[32,33]. Statistical mechanics also predict in that case that the interface between the two regions of homogenized potential vorticity should be minimal, just as bubbles in usual thermodynamics. A key assumption for these results is that the $q - \psi$ relation of the equilibriums state has a tanh-like shape. In the case of an initial distribution $\gamma(\sigma)$ with only two levels of potential vorticity, it can be shown than the $q - \psi$ relation is given exactly by a tanh function[12]. Bouchet and Sommeria [12] conjectured that there exist a much larger class of initial energy E and of fine-grained potential vorticity distributions $\gamma(\sigma)$ that leads to a tanh-like shape for the $q - \psi$ relation at equilibrium. Our phenomenological arguments above and our numerical results below suggest that the dynamics is indeed attracted toward a quasi-stationary state characterized by such a tanh-

like relation in a case where the initial distribution of potential vorticity levels is far from a double delta function, see Fig. 1.

IV. NUMERICAL RESULTS

A. Numerical settings

Quasi-geostrophic simulations are performed using the same numerical model as in Nadeau and Straub[34]. No normal flow and slip conditions are imposed at lateral walls. We use third order Adams-Bashforth scheme for time derivatives, center differencing in space, Arakawa[35] for the Jacobian, and a multigrid method for the elliptic inversions. Momentum conservation is achieved following a procedure similar to that of McWilliams, Holland, and Chow[36], using the zonal momentum equation integrated over a latitude circle in the channel.

To trigger the instability, we considered an initial streamfunction perturbation given by a random velocity field with random phases and a gaussian spectrum of width $\Delta k = 2$ and peaked at $k = 6$; the perturbation where such that $\Psi_1^{init} k \ll U$. As we will see in the high bottom friction limit, the dynamics required thousands of eddy turn-overtime, hence the moderate horizontal resolution. The initial condition for the potential vorticity fields q_1, q_2 is represented on Fig. 1.

There are five adimensionalized parameters in this problem: the adimensisonalized bottom friction coefficient rR/U, the aspect ratio L_x/L_y, the adimensionalized internal Rossby radius of deformation R/L_y, the ratio δ of the upper layer depth with the total depth, and the Reynolds number based on the small scale dissipation coefficient A_h. The small scale dissipation coefficient is adjusted to the lowest necessary value to ensure convergence of the simulation for a given resolution. Arbic and Flierl[8] did show that the result of such simulation does not depend strongly (at least qualitatively) on the form chosen for the small scale dissipation term. We also checked that our results were not dependent on the chosen resolution. Consistently with the exponential stratification observed in most parts of the oceans, we consider that the upper layer is thin compared to the lower layer, with $\delta = 0.2$, and this parameter will be constant for all the simulations. This choice is also reasonable to test the scaling predictions obtained for $\delta \ll 1$. There remains three parameters. The main control parameter is rR/U which is varied from 0 to 40, in order to test our scaling

Parameter	Value
Imposed velocity	$U = 1\text{m.s}^{-1}$
Channel width	$L_y = 900\text{km}$
Fractional depth of the upper layer	$\delta = 0.2$
Rosby radius	$R/L_y = 0.1$
Channel aspect ratio	$L_x/L_y = 5/3$
Bottom friction coefficient	rU/R from 0 to 40
Horizontal resolution	$\Delta x = \Delta y = 1.7\text{km}$
Bi harmonic dissipation coefficient	$A_h = 1.10^8\text{s}^{-1}\text{m}^4$

TABLE I. Model parameters for the reference simulations. Other simulations have been performed by varying R/L_y and Lx/L_y.

predictions obtained for $rR/U \ll 1$ and $rR/U \gg 1$. We considered a ratio $R/L_y = 0.1$ for the reference case (which corresponds to $\delta^{1/2}R/L_y = 0.004$) but also looked at the effect of decreasing this parameter. In any case this parameter can be considered to be much smaller than one. We finally considered aspect ratio $L_x/L_y = 5/3$ for the reference case, which corresponds to a grid $897X513$ in physical space. We explored the effect of varying the domain aspect ratio, but always in the regime $L_y \sim L_x$. These parameters are summarized in table I.

B. The role of bottom friction

1. Energy decay and potential vorticity homogenization

We first discuss reference simulations for which the aspect ratio is $L_x/L_y = 5/3$ and the Rossby radius is $R/L_y = 0.1$. We present Fig. 2 the temporal evolution of the total kinetic energy $KE_{tot} = KE_{1tot} + KE_{2tot}$ and of the total available potential energy APE_{tot} defined Eq. (15), for various values of the bottom friction coefficient rR/U. We see that in any case, the total available potential energy APE_{tot} decreases and eventually vanish. We distinguish three regime for the temporal evolution of the kinetic energy KE_{tot}

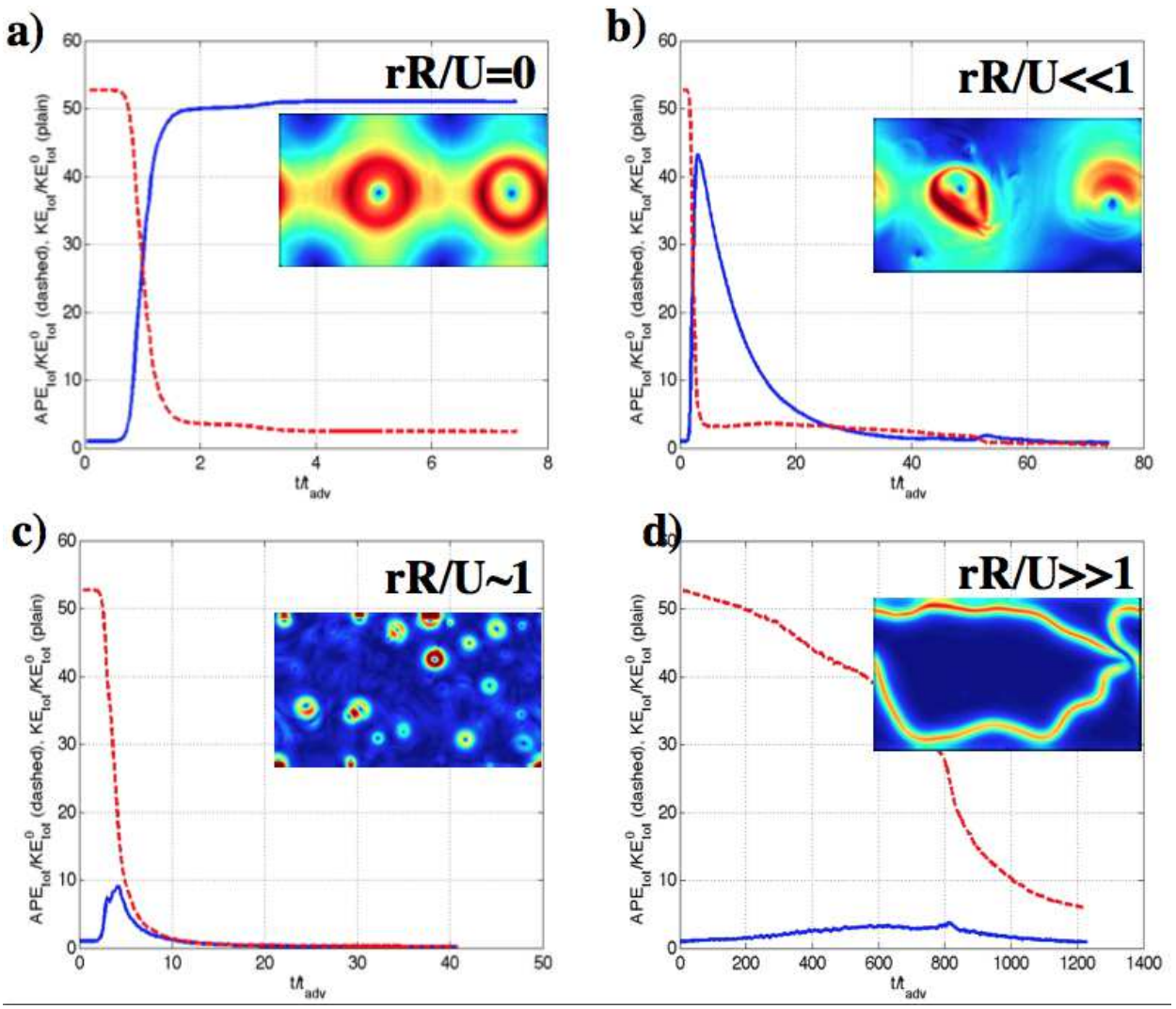

FIG. 2. a) Temporal evolution of the total kinetic energy KE_{tot} and of the total potential energy APE_{tot} in the case rR/U. Time unit is normalized by $t_{adv} = L_y/U$. The field in inset represents a snapshot of the velocity modulus during the kinetic energy decay. b) idem $rR/U = 0.004$ c) idem for $rR/U = 0.5$ d) idem for $rR/U = 40$. Note that the flow structures in each regime are similar to Fig. 7 of Arbic and Flierl[9].

1. the initial growth of KE_{tot}

2. the saturation regime where KE_{tot} reaches its maximal value

3. the decay of KE_{tot} due to bottom friction (except when when $rR/U = 0$).

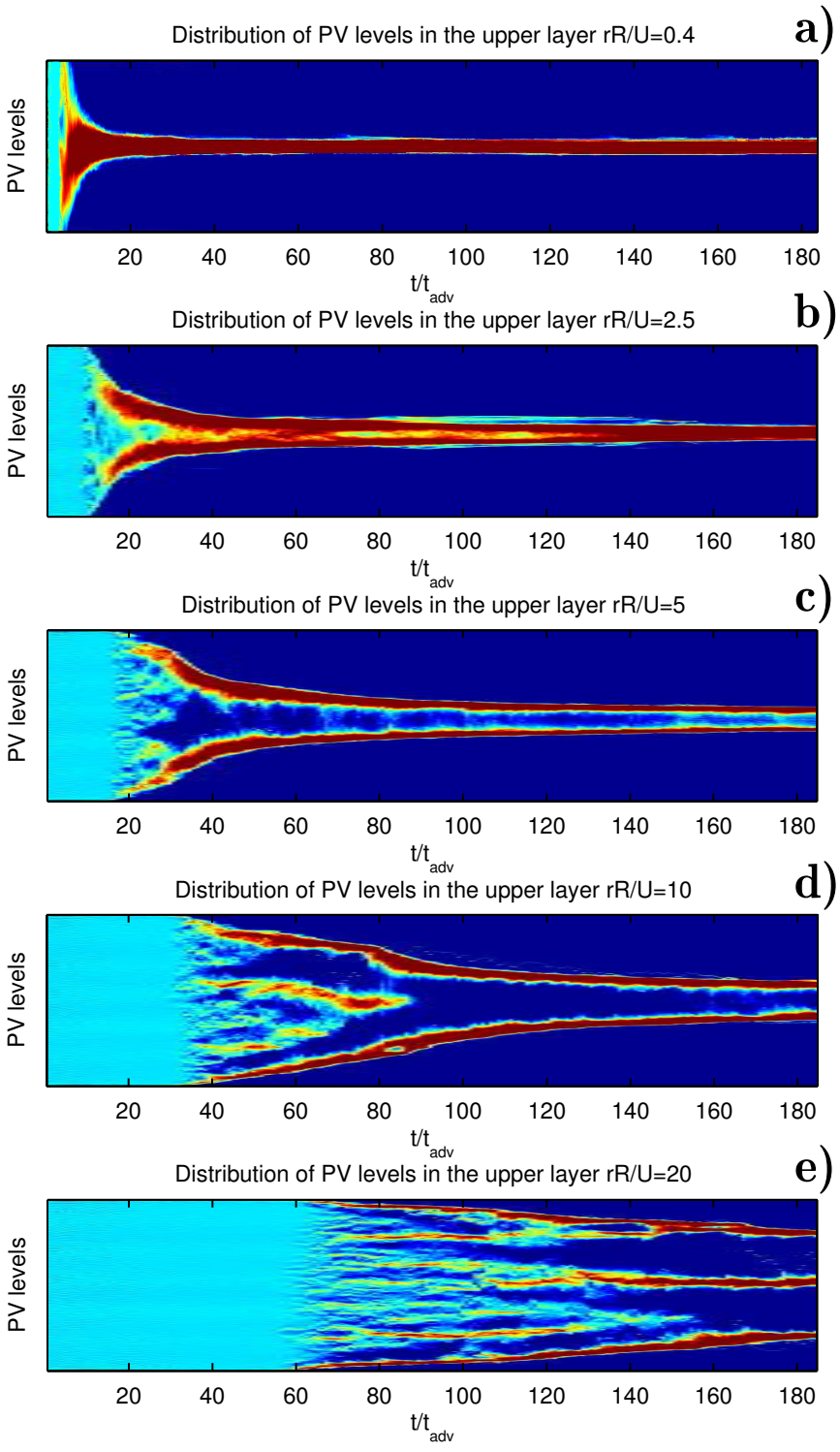
Distribution of PV levels in the upper layer rR/U=0.4
a)
PV levels
20 40 60 80 100 120 140 160 180
t/t_adv
Distribution of PV levels in the upper layer rR/U=2.5
b)
PV levels
20 40 60 80 100 120 140 160 180
t/t_adv
Distribution of PV levels in the upper layer rR/U=5
c)
PV levels
20 40 60 80 100 120 140 160 180
t/t_adv
Distribution of PV levels in the upper layer rR/U=10
d)
PV levels
20 40 60 80 100 120 140 160 180
t/t_adv
Distribution of PV levels in the upper layer rR/U=20
e)
PV levels
20 40 60 80 100 120 140 160 180
t/t_adv

FIG. 3. Routes towards potential vorticity homogenization depending on bottom friction. Each panel represents the temporal evolution of the global distribution of potential vorticity levels in the upper layer. Time is adimensionalized by $t_{adv} = U/L_y$.

As explained before, the decay of the total energy to zero indicates the potential vorticity field is fully homogenized, so that the perturbation has cancelled the effect of the imposed mean flow. Remarkably, the different routes towards complete homogenization and the time scales associated with it are completely different depending on the value of rR/U, which appears clearly on the temporal evolution of the global distribution of potential vorticity levels in the upper layer, see Fig. 3. The observed flow structures during this energy decay also strongly depends on the coefficients rR/U as shown on the insets of Fig. 2. In the weak friction case, the flow is a large scale dipolar vortex condensed at the domain scale. In the large bottom friction limit the flow is a ribbon of kinetic energy of width given by $\delta^{1/2}R$, and in the intermediate bottom friction limit the flow is made of isolated vortex whose size is of the order of the Rossby radius of deformation R. We note that all these flow configurations are qualitatively similar to the one reported in the doubly periodic case by Arbic and Flierl[9].

2. Estimate for the dissipation time

We compare on Fig. 4-a the temporal evolution of the total kinetic energy KE_{tot} for various values of rR/U. Clearly, the time scales for this temporal evolution strongly depend on the value of rR/U. Let us first discuss the initial energy growth. It is a classical result that in the weak friction regime $rR/U \ll 1$ the typical time for baroclinic instability scales as R/U, hence the initial collapse of all the curves that belong to this regime on Fig. 4-a. For the same reason, the saturation of the instability due to self-organization following turbulent stirring always occurs at a time scale of the order of the advection time $t_{adv} = L_y/U$ in this low friction regime. By contrast, in the high friction limit $rR/U \gg 1$, a direct computation of the linear baroclinic instability would show that this instability increases linearly with the bottom friction coefficient r. In addition, our estimate for the non-linear growth of the energy of the perturbation (see the end of subsection III B) lead to a time t_{diss} that also scales linearly with the bottom friction coefficient r. These predictions agrees qualitatively with the fact that kinetic energy peaks occurs at larger time with increasing bottom friction coefficient r on Fig. 4-a.

We focus now on the kinetic energy decay. For a given value of the parameter rR/U, we estimate on Fig. 4-b the decay time t_{diss} as the time interval between the kinetic energy maximum KE_{max} and $KE_{max}/4$. We see that the predictions for this dissipation time given

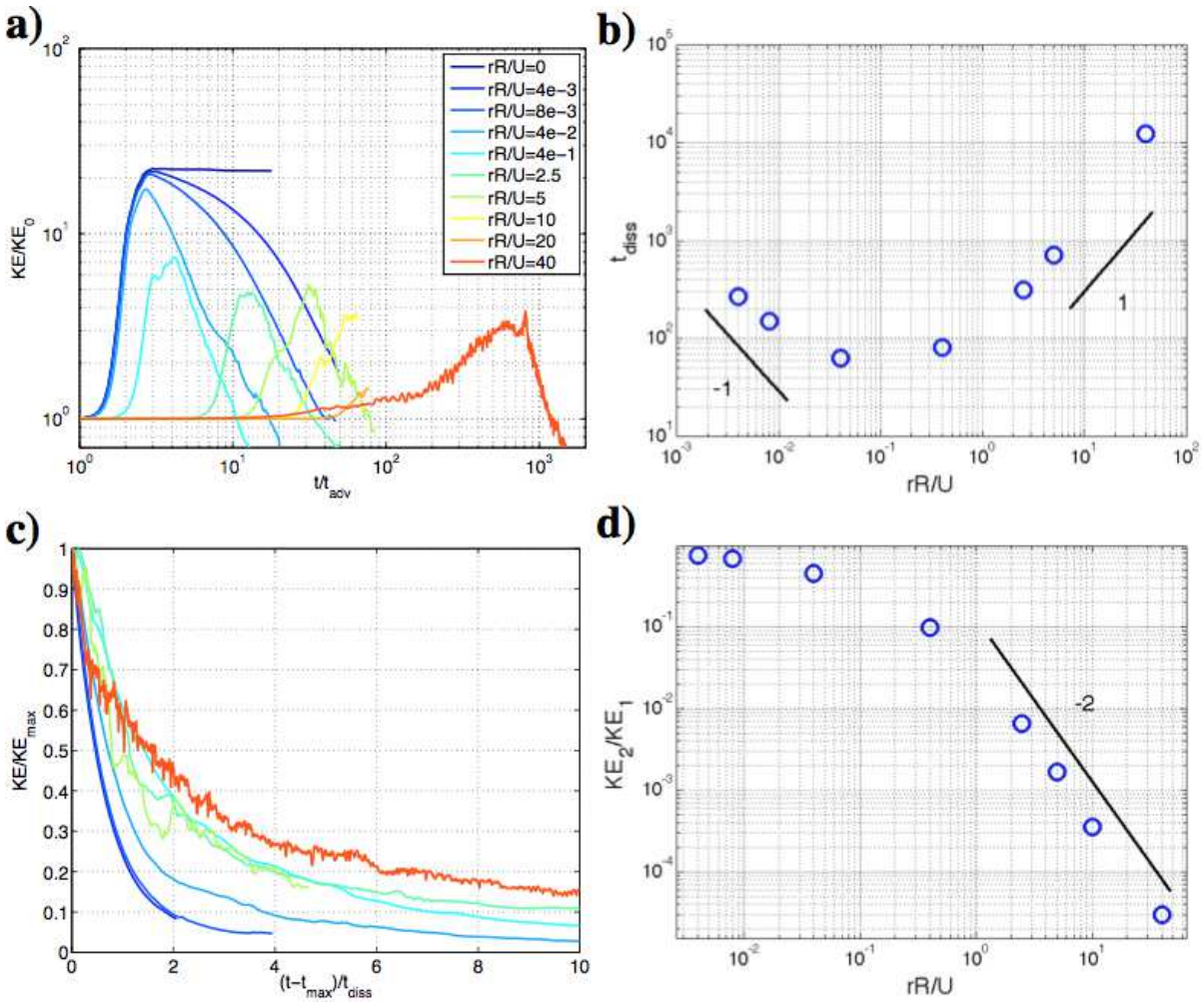

FIG. 4. a) Temporal evolution of the total kinetic energy $KE = KE_1 + KE_2$. The kinetic energy is normalized by its initial value, and the time scale is normalized by the advection time $t_{adv} = L_y/U$. The logarithm scale is used in order to see all the runs on the same plot. b) Estimation of the dissipation time in the numerical experiment (see text for details). c) Temporal decay of the kinetic energy KE_{tot}. The time series are the same than on panel a, but the KE_{tot} is normalized for each run by its maximum value, time coordinate is normalized by the dissipation time defined Eq. (17-18), and the time origin has been translated for each run so that $t = 0$ corresponds to the time where the kinetic energy is maximal.

by Eq. (17-18) yields a good qualitative understanding of the numerical simulations in the low bottom friction regime ($t_{diss} \sim 1/r$) and the large bottom friction regime ($t_{diss} \sim r$). In order to test in more details these predictions for the energy dissipation time scale, we plot

on Fig. 4-c the temporal evolution of the kinetic energy starting from t_{max}, the time when the maximum total kinetic energy has been reached, by renormalizing time unit with the dissipation time t_{diss} given by (17-18), for each value of the parameter rR/U. Remarkably, and despite the four decades range for rU/R, all the curves for the energy decay collapse qualitatively well. This good collapse confirms that not only the scaling obtained in the limit cases are correct, but prefactors are also qualitatively correct.

3. Vertical flow structure

We show on Fig. 4-d the ratio $\delta KE_{2tot}/(1-\delta)KE_{1tot}$ of the total kinetic energy in each layer normalized by the depth of these layers, as a function of the parameter rR/U. We expect from subsection III A that this energy ratio tends to one when $rR/U \ll 1$, i.e. that the flow has become barotropic. We expect from the scaling Eq. (27) that this energy ratio should scale as $\sim (rR/U)^{-2}$ for large rR/U. We see a very good agreement between these predictions and our our numerical results on Fig. 4-d. We stress that both scalings are based on the fact that the flow is self-organized into a quasi-stationary states. This contrasts with the scaling $\delta KE_{2tot}/(1-\delta)KE_{1tot} \sim (rR/U)^{-4/3}$ proposed by Arbic and Flierl[9] by revisiting a cascade argument by Held and Larichev[37]. We believe that their scaling is relevant to describe the vertical structure of the flow for $rR/U \gg 1$ provided that the potential energy length scale remains smaller than the domain size. Since the potential energy length scale increases with rR/U, this scaling should break at some point. In any case, both our scaling and the scaling of Arbic and Flierl[9] predict that the dynamics is well described by a 1-1/2 quasi-geostrophic model in the limit of large frictions $rR/U \gg 1$, and by a barotropic flow model in the low friction limit $rR/U \ll 1$. The next two subsections are devoted to the description of the flow structure in both regimes.

C. Weak friction limit

We see Fig. 2-a that the flow reaches a stationary state when $rR/U = 0$. We checked that in this state, 80% of the kinetic energy was in the barotropic mode, which is in agreement with the fact that barotropization is expected with corrections of order δ or R/L_y when $rR/U \ll 1$ and $\delta \ll 1$, see the discussion subsection III A. We also note that the initial

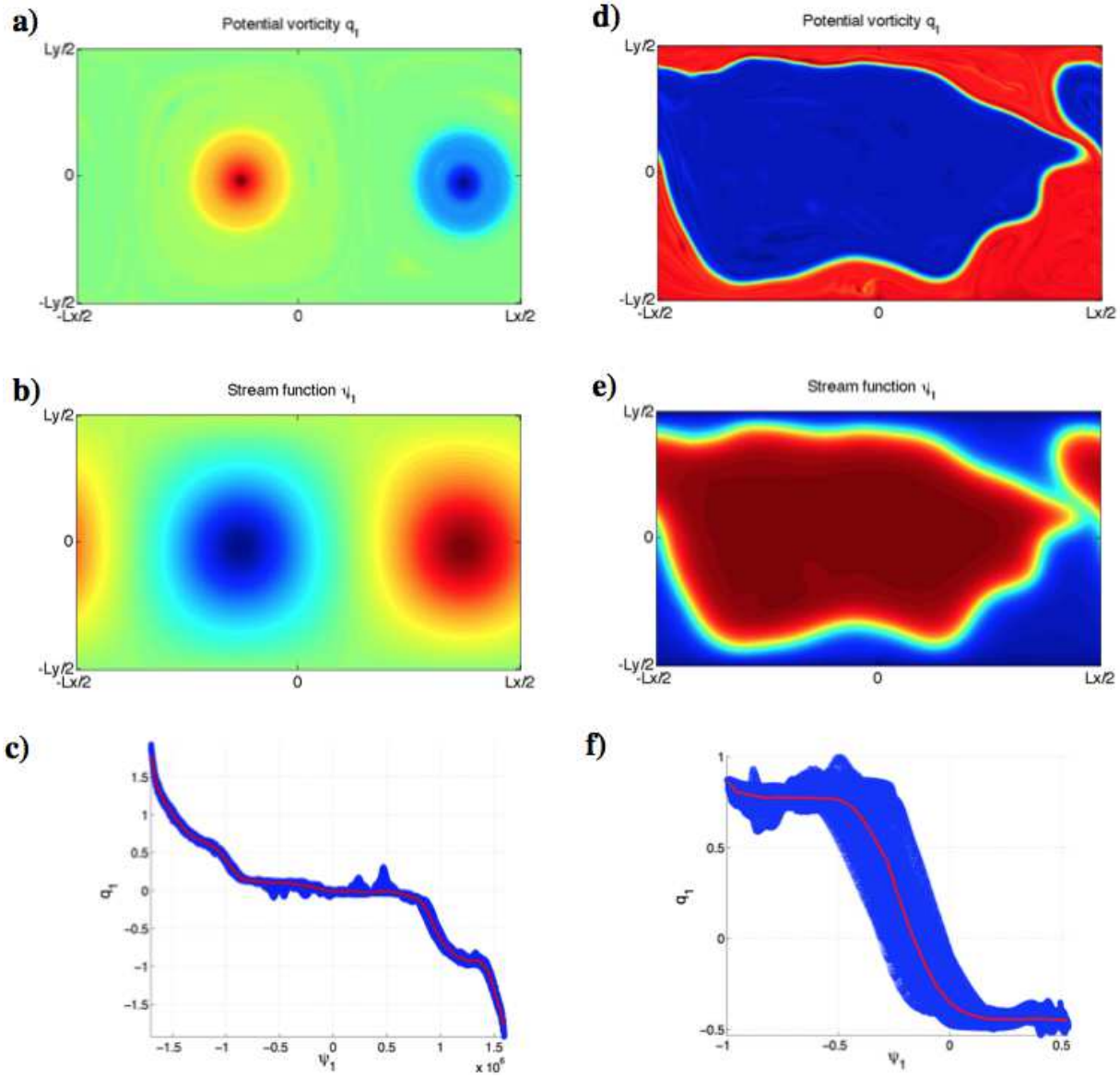

FIG. 5. a) Potential vorticity field in the upper layer for $rR/U = 0$. b) corresponding stream-function field in the upper layer c) scatterplot of the $q - \psi$ relation associated with a and b. d,e,f) same plots in the case with large bottom friction $rR/U \ll 1$.

potential energy reservoir of the baroclinically unstable mean flow ($APE^0_{tot} \gg KE^0_{tot}$) has been transferred almost totally into kinetic energy, due to the conservation of the total energy $E_{tot} = APE_{tot} + KE_{tot}$. We see Fig. 5-a,b that the corresponding large scale streamfunction and potential vorticity fields are self-organized into a dipolar structure at the domain scale. This dipole is characterized by a monotonous relation between potential

vorticity and streamfunction. This functional relation has roughly a sinh shape. This sinh shape is different than the linear $q-\psi$ relation that one would expect in a low energy limit for a initial prescribed potential vorticity distribution. We explained subsection III D 1 that the total energy in the numerical experiment is much smaller than the maximal admissible energy with the same initial global distribution of potential vorticity levels. The reason why a linear $q-\psi$ relation is not observed here is that the core of the remaining vortices have not been stirred during the turbulent evolution of the flow. This shows a lack of ergodicity for the dynamics, which has been discussed for instance by Schecter et al. [38]. However, we note that the observed dipolar structure is the flow that would be predicted by the MRS theory applied to the barotropic model in a channel sufficiently stretched in the x-direction, as explained in subsection III D 1.

In the presence of a weak bottom friction ($rR/U \ll 1$) the large scale state becomes quasi-stationary and the total kinetic energy decreases with a time scale of the order of $1/r$ until the total energy vanish. By quasi-stationary me mean that there still exist a well defined $q-\psi$ relation, but with superimposed small fluctuations that increase when bottom friction increases. The total energy decay goes with the homogenization of the potential vorticity fields. This route towards potential vorticity homogenization is illustrated Fig. 3-a. We see on this figure the rapid emergence of one broad central peak for the global potential vorticity distribution, which indicates that the background potential vorticity field is well mixed over a time $t_{adv} \sim L_y/U$, and the width of the peak decreases more slowly, over a time scale of the order of $1/r$. we also remark that two isolated peaks with large potential vorticity value persists until $t_{diss} \sim 1/r$. These peaks correspond to the unmixed core of the dipolar structure. The increase of their strength is an artifact due to the use of a biharmonic dissipation operator. This would not occur with viscous dissipation.

We note that this route towards complete potential vorticity homogenization and dissipation of the energy of the initial baroclinically unstable mean flow is very much like the classical scenario for two-layer baroclinic turbulence: the instability leads to an inverse energy cascade on the horizontal, with barotropization on the vertical, and then bottom friction dissipates the energy of the large scale flow[5,6].

When the bottom friction is further increased, the inverse energy cascade is arrested before the flow self-organizes at the domain scale, and the number of vortices increases. When rR/U is of order one, the bottom friction time scale $\sim 1/r$ is of the order of the

linear baroclinic instability time scale R/U. One expects therefore that flow structures can not grow larger than the scale of injection, which is the scale of the most unstable mode for linear instability and secondary instabilities, of order R. This explains the formation of coherent structures of size R on Fig. 2-c. These eddies rapidly mix the background potential vorticity field, on the advection time scale $t_{adv} = L_y/U$, as seen on Fig. 3-b. This is a strongly out-of-equilibrium regime, that can not be described by MRS equilibria. In the doubly periodic case, this regime of vortex kinetics can be statistically steady, and has been studied in detail by Thompson and Young[7]. In the case of the channel the number of isolated vortices decreases with time until the potential vorticity field is fully homogenized.

D. Large friction limit

1. Emergence of the ribbons

A typical snapshot of the potential vorticity field when a quasi-stationary state is reached is presented Fig. 5-d for the case $rR/U = 40$. Clearly, at sufficiently large time, the flow has reached a state characterized by two regions of homogenized potential vorticity separated by a sharp interface. By sharp we mean that the interface between the homogenized regions is much smaller than the Rossby radius of deformation of the upper layer $\delta^{1/2}R$. This sharp interface in the potential vorticity field induces typical variations of streamfunction at scale $\delta^{1/2}R$ in the transverse direction, see Fig. 5-e. The scatterplot of the potential vorticity field and streamfunction field is plotted on Fig. 5-f, and shows a tanh-like shape for the $q_1 - \psi_1$ relation. The red line is the averaged potential vorticity along one streamline. The presence of fluctuations around this red line indicates that contrary to the case $rR/U = 0$, the large scale flow is not exactly a stationary states: the interface meanders intermittently break, and the blobs of potential vorticity exchanged during these breaking events are then stretched and folded in each region of homogenized potential voracity, hence the presence of potential vorticity fluctuations.

It is notable that the dynamics drives the system towards a state characterized by a 'tanh' relation between vorticity and streamfunction, given that the initial potential vorticity field in the upper layer is a gradient in the meridional direction presenting no region of homogenized potential vorticity. In that respect, our results support for the the claim of[12]

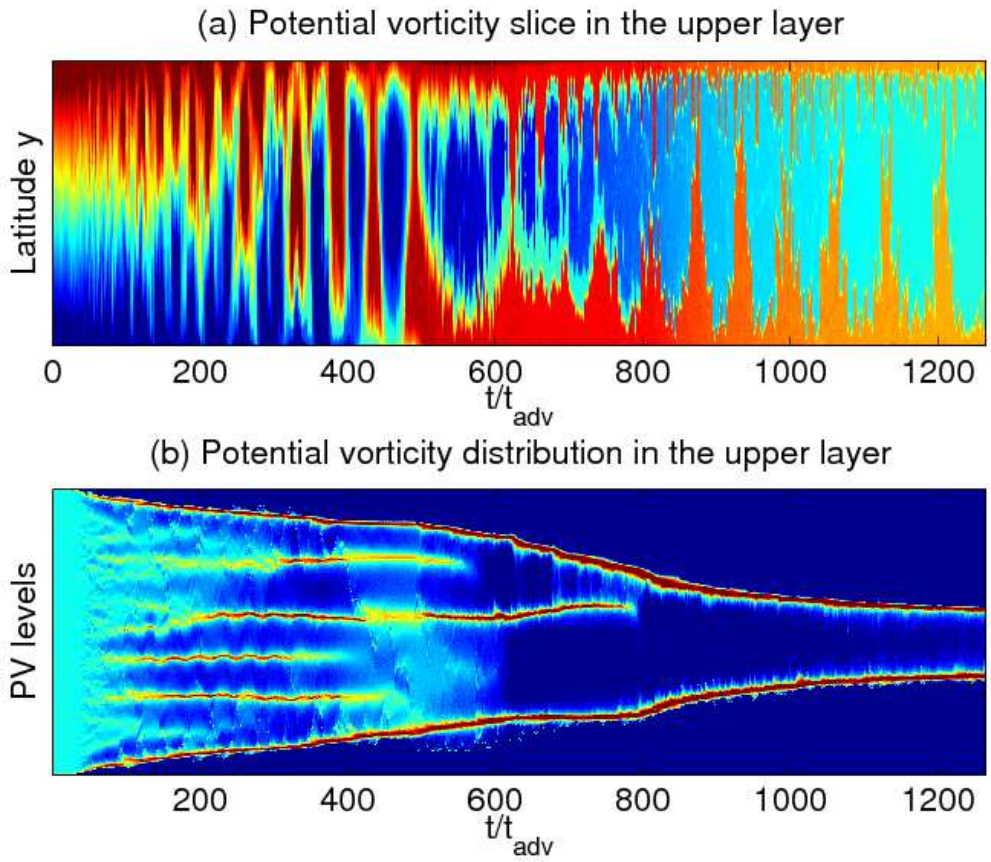

FIG. 6. a) Hovmöller diagram of a potential vorticity line q(y,t) for a given longitude x. b) Temporal evolution of the global distribution of potential vorticity levels. Time is adimensionalized by $t_{adv} = U/L_y$ in both cases. .

that phase separation of the potential vorticity field into two homogenized regions is a generic feature of 1-1/2 layer quasi-geostrophic equilibria, that does not depend on the particular initial condition when $\delta^{1/2} R/L_y \ll 1$.

The spontaneous emergence of ribbons also support the argument of subsection III C based on cascade phenomenology and on potential vorticity homogenization theory. Indeed, we see Fig. 7 a comparison between the temporal evolution of the kinetic and potential energy centroids both in the case $rR/U = 0$ (barotropic dynamics at lowest order) and $rR/U = 40$ (1-1/2 layer quasi-geostrophic dynamics at lowest order). In the case with vanishing bottom friction, the kinetic energy centroid goes to the domain scale and remains there, as expected from inverse energy cascade arguments. In the case with high bottom friction, the centroids of potential energy initially goes to large scale, and so does the cen-

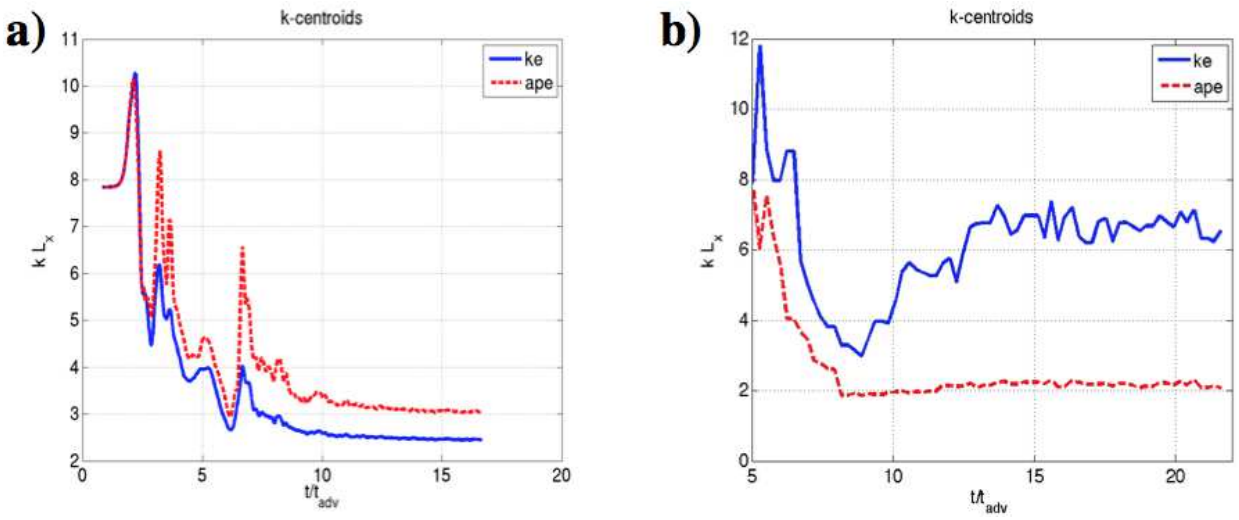

FIG. 7. a) Initial temporal evolution of the barotropic kinetic energy k-centroid $k_{KE} = \int dk\ k\widetilde{KE}_t(k)/\int dk\ \widetilde{KE}_t(k)$ and of the available potential energy centroid $k_E = \int dk\ k\widetilde{APE}(k)/\int dk\ \widetilde{APE}(k)$ in the case $rR/U = 0$. b) Initial temporal evolution of the kinetic energy k-centroid of the upper layer and of the available potential energy k-centroid in the case $rR/U = 40$. Time is adimensionalized in both case by $t_{adv} = L_y/U$.

troids of kinetic energy (slaved to the inverse cascade of potential energy). But once these centroids have reached the domain scale, the kinetic energy centroids goes back to smaller scale until a plateau is reached, while the potential energy centroids remains to large scale. This clearly indicates that streamlines are "pinched", or expelled at the boundary between regions of homogenized potential vorticity. It was shown by Dritschel and Scott [39] that such jet sharpening mechanism through turbulent stirring is enhanced by the presence of coherent vortices in the vicinity of the jets. We actually observed the presence of such vortices for values of bottom friction rR/U large but of order one, but these vortices disappeared at large time for $rR/U > 10$.

The emergence of the ribbons as a potential homogenization process is conveniently described by a Hovmöller diagram of Fig. 6-a showing the temporal evolution of meridional slice of the potential vorticity profile $q_1(y,t)$, and by the temporal evolution of the global distribution of potential vorticity levels shown Fig. 6-b. Clearly, the dynamics initially form multiples regions of homogenized potential vorticity with ribbons at their interface, and these regions eventually merge together until two regions of homogenized potential vorticity

are formed.

2. Ribbon dynamics

We explained in subsection III D 2 that statistical mechanics theory of the 1-1/2 layer model with small R/L_y predicts not only the ultimate formation of two regions of homogenized potential vorticity, but also the organization of these regions into a configuration that minimizes the length of their interface. Clearly, the interface perimeter of the potential vorticity field in Fig. 5-d is not minimal. Moreover, a movie would reveal that this interface is permanently meandering, and sometimes even breaks locally. Indeed, the jets at the interface between the regions of homogenized potential vorticity field are characterized by a strong vertical shear, and are therefore expected to be baroclinically unstable. This instability is actually a mixed barotropic-baroclinic instability, since the jets have an horizontal structure. To check that the meanders were due to the existence of a vertical shear, we ran a numerical simulation of the 1-1/2 quasi-geostrophic dynamics taking the potential vorticity field of Fig. 5-d as an initial condition. This amounts to impose $\psi_2 = 0$, and therefore precludes any baroclinic instability. In those freely evolving simulations the interface did stop meandering and the flow did reach a stationary state. We also observed that the interface was eventually smoothed out in the freely evolving 1-1/2 layer quasi-geostrophic simulations, while the interface remains sharp throughout the flow evolution when baroclinic instability is allowed, as seen on the Hovmöller diagram 6-a. We conclude that in the limit of large bottom friction, there is a competition between baroclinic instability that tends to increase the interface perimeter between regions of homogenized potential vorticity, and the dynamics of the inviscid 1-1/2 layer quasi-geostrophic dynamics that tends to minimize this interface.

Baroclinic instability of the ribbons is the mechanism that allows to reduce little by little the potential vorticity jumps across the ribbons, at a time scale given by $t_{diss} \sim rRL_y/(\delta^{1/2}U^2)$. This time scale is of the order of the slow variations of the potential vorticity interface at large time in the Hovmöller diagram 6-a. We see on Fig. 6 that once two regions of homogenized potential vorticity are formed, the value of the potential vorticity jump $\mathcal{Q}_{1jump}$ between the homogenized regions decreases exponentially, with an e-folding depth of the order of the decay time for the kinetic energy t_{diss}. The corresponding flow

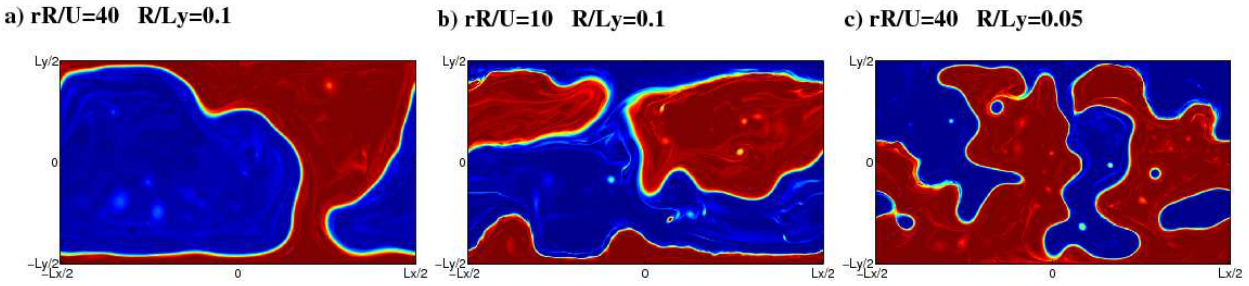

FIG. 8. Typical snapshots of the potential vorticity field a) in the reference case b) when bottom friction coefficient rR/U is decreased c) when the Rossby radius R/L_y is decreased. The typical size of the potential vorticity blobs decreases from a to c and the interface perimeter increases from a to c.

structure (i.e. meandering jets with a ribbon shape) remains the same, but the strength of the jet also decreases in time, since $U_{jet} \sim \delta^{1/2} R\mathcal{Q}_{1jump}$.

3. A competition between interface minimization and baroclinic instability

We show on Fig. 5-d a case where two simply connected regions of homogenized potential vorticity are formed. When bottom friction is decreased from $rR/U = 40$ to $rR/U = 2$, we see on the histograms of potential vorticity levels Fig. 3 that the global potential vorticity distribution still evolves to a state characterized by a double delta function. However, a snapshot of the potential vorticity field Fig. 8-b reveals that when rR/U is decreased, the two peaks in the potential vorticity distribution are associated with several unconnected blobs of regions with homogenized potential vorticity. The typical size of potential vorticity blobs decreases with lower bottom friction, while the total interface perimeter increases with lower bottom friction. Similarly, we observed that decreasing the ratio R/L_y for a given value of the bottom friction coefficient lead to an increase of the interface perimeters between region of homogenized potential vorticity, and to favor the detachment of isolated blobs of homogenized potential vorticity, see Fig. 8-c.

We interpret these observations by noting first that destabilization of the ribbons occurs at a time scale of the energy decay controlled by the baroclinic instability, and given by $t_{diss} \sim (rRL_y/U^2)$ according to the large friction limit of Eq. (17-18). By contrast,

the tendency of the 1-1/2 quasi-geostrophic dynamics to form simply connected regions of homogenized potential vorticity with minimal interface occurs at a time scale t_{relax} independent from bottom friction parameter rR/U. To estimate t_{relax}, we assume first that the flow is composed of two "phases" characterized by different values of potential vorticity, but that there are several blobs associated with each phase (like bubbles in liquid water). The potential vorticity jump between these two phases can be estimated to be initially $\mathcal{Q}_1 \sim UL_y/\delta R^2$, which corresponds to stream function variations $\psi_1 \sim UL_y$. Let us introduce L_{flow} the typical length scale of a blob of homogenized potential vorticity. Then, assuming $L_{flow} \gg \delta^{1/2}R$ and $L_{flow} \ll L_y$, and using the fact that the dynamics of the large scale flow is given at lowest order by the planetary quasi-geostrophic model Eq. (33), we obtain $\partial_t\psi_1/(\delta R^2) \sim J(\nabla^2\psi_1, \psi_1)$, which gives $UL_y/(t_{relax}\delta R^2) \sim (UL_y)^2/L_{flow}^4$. A quasi-stationary state is reached when the relaxation time scale is of the order of the baroclinic instability time scale ($t_{relax} \sim t_{diss}$), which yields

$$L_{flow} \sim L_y \left(\frac{rR}{U}\right)^{1/4} \left(\frac{R}{L_y}\right)^{1/2} \delta^{1/8}. \tag{34}$$

The validity of scaling requires a scale separations that was not clear in our simulations (the potential vorticity blobs are not much smaller than the domain scale on Fig. 8). However, this naive scaling allows to interpret qualitatively our numerical results. The main point is that decreasing the bottom friction or the Rossby radius of deformation corresponds to a decrease of the typical size of L_{flow} isolated blobs of potential vorticity, which means an increase of the number of isolated blobs (since the goal area of a given phase is fixed), and therefore an increase of the total interface perimeter. We also note that the exponent 1/4 means that variations of L_{flow} are very weak when bottom friction is changed over one or two decades such as in our simulations. Finally, we note that the length scale L_{flow} for the homogenized potential vorticity blobs can be interpreted as the scale of the available potential energy field, and that our scaling Eq. 34 is in very good agreement with the variations of the potential energy centroids when bottom friction is varied in numerical simulation by Arbic and Flierl[9] (figure 9-a of their paper).

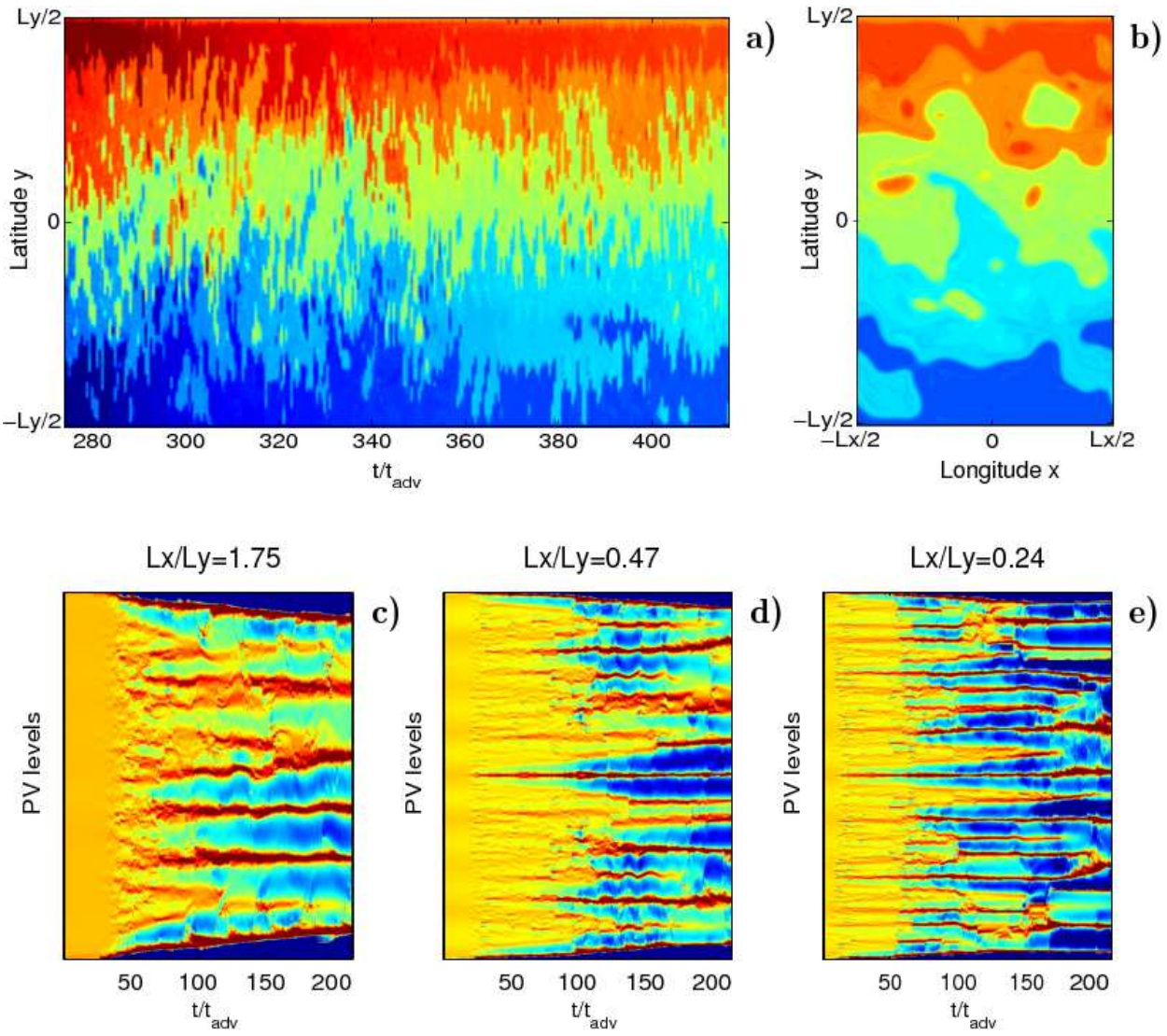

FIG. 9. Multiple jets as a transient regime towards complete homogenization. a) Hovmöller diagrams of a meridional slice of the potential vorticity field in the upper layer, time unit is $t_{adv} = L_y/U$. b) Typical snapshot of the potential vorticity field in the upper layer. c), d) and e) Evolution of the global distribution of potential vorticity levels in the upper layer for different values of the domain aspect ratio, L_x/L_y =1.75, 0.47 and 0.24 respectively.

4. Multiple jets

We see on Fig. 6-b that there is a transient regime with multiple peaks in the global potential vorticity distribution. These transient states correspond initially to multiple regions of homogenized potential vorticity. We found that in the ribbon regime, the number

of long lasting multiple regions of homogenized potential vorticity increased: i/ when the domain aspect ratio L_x/L_y was decreased, ii/ when bottom friction rR/U was increased and iii/ when the parameter R/L_y was decreased. In addition, when the parameter R/L_y was sufficiently small, the regions of homogenized potential vorticity are initially organized into zonal bands with east jet at their interface, which is reminiscent of potential vorticity staircases[40]. We in show Fig 9-a,b an example of such long lasting multiple zonal bands of potential vorticity. In addition, Fig 9-c,d,e show how the number of regions of homogenized potential vorticity increases with smaller domain aspect ratio L_x/L_y. It is not clear wether the dynamics would eventually form only two regions of homogenized potential vorticity, or if more than two regions of homogenized potential vorticity could last for ever. One may interpret qualitatively the emergence of these zonal potential vorticity staircases by noticing that once a jet is formed between two regions of homogenized potential vorticity, it acts as a strong mixing barrier between the two adjacent regions, which may prevent further mixing with other regions of homogenized potential vorticity. We note that in our case there is no beta effect. The zonal organization of the potential vorticity field only reflects the structure of the imposed mean flow, which induces an effective beta effect in the upper layer.

The existence of long lived multiple eastward jets provides a route towards potential vorticity homogenization that sustains a total eastward transport of the order of the transport of the imposed mean flow. This contrasts with the low or intermediate bottom friction case where the rapid decrease of the total potential energy (over a time $t_{adv} = L_y/U$) is accompanied with a rapid decrease of the total zonal transport. In that respect we find that increasing bottom friction leads to an increasing zonal transport in the regime where multiple jets are allowed. Increasing transport associated with increasing bottom friction was reported in the context idealized simulations of the antarctic circumpolar circulation[41], but this effect was due to the presence of bottom topography which is absent in our simulations.

V. CONCLUSION

We have presented numerical simulations for the non-linear equilibration of a two-layer quasi-geostrophic flow in a channel in the presence of a baroclinically unstable imposed mean flow U in the upper layer with particular attention to the role of bottom friction. For any non zero value of the bottom friction coefficient, r, the dynamics attempts to homogenize

the potential vorticity field, including any large scale gradient due to imposed mean flow, as might expected from classical theories of geostrophic turbulence[42]. This leads eventually to a perturbed flow that annihilates the imposed mean flow. However, the route toward complete homogenization depends strongly on the bottom friction coefficient.

When the bottom friction is weak ($r \ll U/R$), the perturbation self-organizes at the domain scale into a quasi-barotropic large scale structure (see movie 1 in supplementary materials), which is then weakly dissipated on a time scale inversely proportional to the bottom friction coefficient, $t_{diss} \sim 1/r$. We interpret this large-scale quasi-stationary flow as a statistical equilibrium state of the Miller-Robert-Sommeria (MRS) theory.

When the bottom friction has a medium value — meaning that its time scale is of the order of the inviscid baroclinic instability time scale ($r \sim U/R$) — bottom friction precludes an inverse kinetic energy cascade close to the injection length scale (which is of the order of the Rossby radius deformation R) and the dynamics is well described by a gas of isolated vortices of size R mixing the background potential vorticity field at the advection time scale $t_{diss} \sim L_y/U$ (see movie 2 in supplementary materials).

When the bottom friction coefficient is high ($r \gg U/R$), the ratio between the lower layer kinetic energy and the upper layer kinetic energy scales as $(rR/U)^2$ and the dynamics is well described at lowest order by a 1-1/2 layer quasi-geostrophic model. We observed the spontaneous emergence of meandering ribbons corresponding to strong jets of width given by the Rossby radius of deformation of the upper layer, and separating regions of homogenized potential vorticity (see movie 3 in supplementary materials). We used statistical mechanics arguments as well as cascade phenomenology to interpret these results. We described a competition between the inviscid 1-1/2 quasi-geostrophic dynamics that tends to form only two regions of homogenized potential vorticity with a minimal interface between them, and baroclinic instability of the ribbons that tend to increase the interface perimeter. This last route towards potential vorticity homogenization is rather spectacular: the potential vorticity jump between the two regions of homogenized potential vorticity decreases slowly with time, due to the intermittent breaking of the ribbons at their interface. This process occurs at a time scale given by baroclinic instability that scales linearly with the bottom friction coefficient $t_{diss} \sim rRL_y/U^2$. Remarkably, the interface between the homogenized regions of potential vorticity remains sharp (i.e. much smaller than the Rossby radius of deformation) throughout this evolution towards a single, fully homogenized potential

vorticity field.

Using cascade phenomenology, and generalizing the arguments by Held and Larichev[37], Arbic and Flierl[9] proposed scalings for the horizontal scale and the vertical structure of the dynamics in the large friction regime. Here we obtained rather different scalings, but with similar qualitative meaning, by assuming that the flow structures resulted from the competition between baroclinic instability and a tendency to reach a MRS equilibrium state in both the weak and the large bottom friction limit. We believe that the cascade arguments are more suited to intermediate bottom friction, for which there is a scale separation between the large scale flow and the perturbed flow. A key novelty of our work is to relate the emergence of the ribbons with existing statistical predictions for the 1-1/2 layer quasi-geostrophic model. In particular, we show for the first time numerical evidence that when the Rossby radius of deformation is much smaller than the domain scale, the dynamics attract the system towards a quasi-stationary state characterized by a tanh-like relation between potential vorticity and stream function, even if the initial potential vorticity distribution is not already made of several regions with homogenized potential vorticity. We note that in our case the presence two layers was essential to observe large regions of homogenized potential vorticity, even if the dynamics is described at lowest order by a 1-1/2 layer quasi-geostrophic flow. Indeed, the presence of the bottom layer allows for baroclinic instability of the ribbons, which favors stirring of the upper layer potential vorticity field in the whole flow domain. By contrast, once a ribbon emerges in a freely evolving 1-1/2 quasi-geostrophic flow, it acts as a mixing barriers that prevent further exchanges between adjacent regions of homogenized potential vorticity.

Our work was set in a channel geometry in which case the global distribution of a suitably defined potential vorticity field is conserved in the absence of small scale dissipation. This allows us to use of statistical mechanics arguments and reinterpret the results obtained in previous work in doubly periodic geometry. Thus, in the large bottom friction limit, the dissipation time $t_{diss} \sim rRL_y/U^2$ can be interpreted as an intrinsic time scale for the variability of the available potential energy in a statistically steady state. It is also interesting to compare our results with those of Esler[43], Willcocks and Esler[44] who considered the free evolution of an surface intensified zonal jet localized at the center of a channel. In their case, the instability is localized around the jet, and potential vorticity stirring occurs only within this central region. Statistical mechanics predictions fail in this case to predict the large scale

flow structure since the dynamics does only explore a restricted part of the phase space. By contrast, in our simulations, the initial instability and its subsequent turbulent evolution takes place in the whole domain, which induces potential vorticity stirring everywhere, excepted when multiple jets occur.

To conclude, this study shows that large bottom friction induces the condensation of the kinetic energy into quasi-stationary ribbons and the concomitant condensation of potential energy at large scale. Perhaps paradoxically increasing the bottom friction considerably slows down the loss of energy from the potential energy reservoir associated with the large scale flow.

The regime for ribbons turbulence requires bottom friction coefficient which are too high for a direct application to oceanic flows. However, other physical mechanism than bottom drag may be able to remove energy from the lower layer, which would mimmic the effect of high bottom friction. For instance LaCasce and Brink[45] showed in the framework of freely solving two-layer quasi-geostrophic turbulence over a slope that topographic Rossby waves generated in some location remove the energy to other locations, where it eventually is dissipated by bottom drag. This effect may me interpreted as an enhanced bottom friction in the region where the topographic wave is generated.

Further work will be needed to extend these results to continuously stratified fluids because in that case other effects can significantly change the properties of the vertical structure of the eddies, see Smith and Vallis[46], Roullet et al.[47] for the forced dissipated case, and Smith and Vallis[48] for the freely evolving case. In particular, Smith and Vallis[48], Fu and Flierl[49] did show that in the presence of surface intensified stratification, and without bottom friction, there is a fast time scale associated with energy transfers toward the first baroclinic mode. This energy eventually condense into the barotropic mode, but with a much larger time scale. The beta effect may also have several consequences: it is known to favor barotropization[15], and to favor the arrangement of regions of homogenized potential vorticity into zonal bands.

Finally, we note that we have here considered only an imposed mean flow and it would be useful to generalize to a more realistic forcing by considering a surface wind stress or relaxation towards a prescribed unstable flow. We conjecture that our estimate for the dissipation time t_{diss} will still play an important role to describe low frequency, internal variability of the system, with the only difference that the estimate of the large scale velocity

U will have to be related to the forcing case by case.

a. Acknowledgments

VI. APPENDIX A BAROTROPIZATION IN THE WEAK BOTTOM FRICTION LIMIT

The aim of this appendix is to give a phenomenological argument for barotropization when $R \ll L_y$ or $\delta \ll 1$, with $L_x \sim L_y$. The argument is based on the fact that turbulence leads to a rearrangement of the initial potential field in each layer, with a constant total energy E_{tot}.

The global distribution of potential vorticity levels in both layers are conserved when there is neither small scale dissipation nor bottom friction.

Let us call $\mathcal{Q}_1$ the typical variations of the potential vorticity field in the upper layer after turbulent rearrangement of the initial field $q_1^0 = Uy/(\delta R^2)$. We see Eq. (21) that typical variations of the barotropic streamfunction are given by $\psi_t \sim \delta L_y^2 \mathcal{Q}_1$, where we anticipate that the typical length scale of flow structures in this regime is given by the domain size L_y. We also see from Eq. (20) that typical variations of the baroclinic streamfunction are $(\psi_c - Uy) \sim \delta(1-\delta)R^2\mathcal{Q}_1$ over a length $(\delta(1-\delta))^{1/2}R$ when $(\delta(1-\delta))^{1/2}R \ll L_y$. With these estimates, and anticipating that $\psi_t \gg Uy$, we find the following scalings for the different components of the energy of the perturbed flow introduced Eq. (24):

$$KE_{tot,t} \sim \mathcal{Q}_1^2 L_y^4 \ , \quad KE_{tot,c} \sim \mathcal{Q}_1^2 \delta(1-\delta) R^3 L_y \ , \quad APE_{tot,c} \sim \mathcal{Q}_1^2 \delta^2 R^2 L_y^2 \ . \tag{35}$$

Clearly, the total energy $E_{tot} = KE_{tot,t} + KE_{tot,c} + APE_{tot,c}$ is dominated its barotropic component $KE_{tot,t}$ when $\delta \ll 1$ or $R \ll L_y$. Since the barotropic dynamics leads to an inverse kinetic energy cascade, our hypothesis that L_y is a typical scale of the flow is self-consistent. Using the estimate of the initial energy $E_{tot}^0 \sim APE_{tot}^0 \sim U^2 L_y^4/R^2$, and using the fact that this energy is fully transferred into the barotropic mode after turbulent rearrangement, we get $KE_{tot,t} \sim U^2 L_y^4/R^2$. Using Eq. (35), this estimate yields $\mathcal{Q}_1 \sim U/R$. Consequently, the order of magnitude for the barotropic velocity is $U_t \sim UL_y/R$, which is consistent with the hypothesis that the barotropic flow is dominated by the perturbed flow ($\psi_t \gg \delta Uy$). We conclude that the total flow is dominated by the barotropic component of the perturbed flow when $\delta \ll 1$ or $R \ll L_y$ after turbulent rearrangement of the potential vorticity field.

REFERENCES

[1]I. M. Held, "The gap between simulation and understanding in climate modeling," Bulletin of the American Meteorological Society **86**, 1609–1614 (2005).

[2]A. Colin de Verdiere, "Keeping the freedom to build idealized climate models," EOS **90** (2009), 10.1029/2009EO260005.

[3]G. K. Vallis, Atmospheric and Oceanic Fluid Dynamics (Cambridge University Press, 2006).

[4]J. G. Charney, "Geostrophic turbulence," Journal of the Atmospheric Sciences **28**, 1087–1095 (1971).

[5]P. B. Rhines, "Geostrophic turbulence," Annual Review of Fluid Mechanics **11**, 401–441 (1979).

[6]R. Salmon, Lectures on Geophysical Fluid Dynamics (Oxford University Press, 1998).

[7]A. F. Thompson and W. R. Young, "Scaling Baroclinic Eddy Fluxes: Vortices and Energy Balance," Journal of Physical Oceanography **36**, 720 (2006).

[8]B. K. Arbic and G. R. Flierl, "Coherent vortices and kinetic energy ribbons in asymptotic, quasi two-dimensional f-plane turbulence," Physics of Fluids **15**, 2177–2189 (2003).

[9]B. K. Arbic and G. R. Flierl, "Baroclinically unstable geostrophic turbulence in the limits of strong and weak bottom ekman friction: Application to midocean eddies," Journal of Physical Oceanography **34**, 2257–2273 (2004).

[10]J. Miller, "Statistical mechanics of euler equations in two dimensions," Phys. Rev. Lett. **65**, 2137–2140 (1990).

[11]R. Robert and J. Sommeria, "Statistical equililbrium states for two-dimensional flows," Journal of Fluid Mechanics **229**, 291–310 (1991).

[12]F. Bouchet and J. Sommeria, "Emergence of intense jets and Jupiter's Great Red Spot as maximum-entropy structures," Journal of Fluid Mechanics **464**, 165–207 (2002).

[13]J. Pedlosky, "Geophysical fluid dynamics," New York and Berlin, Springer-Verlag, 1982. 636 p. **1** (1982).

[14]T. G. Shepherd, "Nonlinear saturation of baroclinic instability. part i: The two-layer model." Journal of Atmospheric Sciences **45**, 2014–2025 (1988).

[15]A. Venaille, G. Vallis, and S. Griffies, "The catalytic role of the beta effect in barotropization processes," Journal of Fluid Mechanics **709**, 490–515 (2012).

[16]C. Herbert, "Nonlinear energy transfers and phase diagrams for geostrophically balanced rotating–stratified flows," arXiv preprint arXiv:1310.2280 (2013).

[17]A. Renaud, A. Venaille, and F. Bouchet, "High energy equilibrium states of stratified quasi-geostrophic flows and application to oceanic rings," preprint **000**, 000 (2014).

[18]R. Fjortoft, "On the changes in the spectral distribution of kinetic energy for two-dimensional nondivergent flow," Tellus **5**, 225–230 (1953).

[19]R. H. Kraichnan, "Inertial Ranges in Two-Dimensional Turbulence," Phys. Fluids **10**, 1417 (1967).

[20]S. Nazarenko and B. Quinn, "Triple Cascade Behavior in Quasigeostrophic and Drift Turbulence and Generation of Zonal Jets," Physical Review Letters **103**, 118501 (2009).

[21]V. D. Larichev and J. C. McWilliams, "Weakly decaying turbulence in an equivalent-barotropic fluid," Physics of Fluids **3**, 938–950 (1991).

[22]R. T. Pierrehumbert, I. M. Held, and K. L. Swanson, "Spectra of local and nonlocal two-dimensional turbulence," Chaos Solitons and Fractals **4**, 1111–1116 (1994).

[23]K. S. Smith, G. Boccaletti, C. C. Henning, I. Marinov, C. Y. Tam, I. M. Held, and G. K. Vallis, "Turbulent diffusion in the geostrophic inverse cascade," Journal of Fluid Mechanics **469**, 13–48 (2002).

[24]J. Miller, P. B. Weichman, and M. Cross, "Statistical mechanics, eulers equation, and jupiters red spot," Physical Review A **45**, 2328 (1992).

[25]A. Majda and X. Wang, Nonlinear Dynamics and Statistical Theories for Basic Geophysical Flows (Cambridge University Press, 2006).

[26]J. Marston, "Planetary atmospheres as non-equilibrium condensed matter," arXiv preprint arXiv:1107.5289 (2011).

[27]F. Bouchet and A. Venaille, "Statistical mechanics of two-dimensional and geophysical flows," Physics reports **515**, 227–295 (2012).

[28]V. Lucarini, R. Blender, C. Herbert, S. Pascale, and J. Wouters, "Mathematical and physical ideas for climate science," arXiv preprint arXiv:1311.1190 (2013).

[29]P. Chavanis and J. Sommeria, "Classification of self-organized vortices in two-dimensional turbulence: the case of a bounded domain," Journal of Fluid Mechanics **314**, 267–298 (1996).

[30]A. Venaille and F. Bouchet, "Solvable Phase Diagrams and Ensemble Inequivalence for Two-Dimensional and Geophysical Turbulent Flows," Journal of Statistical Physics **143**,

346–380 (2011).

[31]M. Corvellec, Phase transitions in two-dimensional and geophysical turbulence (PHD, Ecole Normale Superieure de Lyon, 2012).

[32]P. B. Weichman, "Equilibrium theory of coherent vortex and zonal jet formation in a system of nonlinear Rossby waves," Physical Review E **73**, 036313 (2006).

[33]A. Venaille and F. Bouchet, "Oceanic Rings and Jets as Statistical Equilibrium States," Journal of Physical Oceanography **41**, 1860–1873 (2011).

[34]L.-P. Nadeau and D. N. Straub, "Basin and channel contributions to a model antarctic circumpolar current," Journal of Physical Oceanography **39**, 986–1002 (2009).

[35]A. Arakawa, "Computational design for long-term numerical integration of the equations of fluid motion: Two-dimensional incompressible flow. part i," Journal of Computational Physics **1**, 119–143 (1966).

[36]J. C. McWilliams, W. R. Holland, and J. Chow, "A description of numerical antarctic circumpolar currents," Dynamics of Atmospheres and Oceans **2**, 213–291 (1978).

[37]I. M. Held and V. D. Larichev, "A scaling theory for horizontally homogeneous, baroclinically unstable flow on a beta plane," Journal of the atmospheric sciences **53**, 946–952 (1996).

[38]D. Schecter, D. Dubin, K. Fine, and C. Driscoll, "Vortex crystals from 2d euler flow: Experiment and simulation," Physics of Fluids **11**, 905 (1999).

[39]D. Dritschel and R. Scott, "Jet sharpening by turbulent mixing," Philosophical Transactions of the Royal Society A: Mathematical, Physical and Engineering Sciences **369**, 754–770 (2011).

[40]D. Dritschel and M. McIntyre, "Multiple jets as pv staircases: the phillips effect and the resilience of eddy-transport barriers," Journal of the Atmospheric Sciences **65**, 855–874 (2008).

[41]L.-P. Nadeau and D. N. Straub, "Influence of wind stress, wind stress curl, and bottom friction on the transport of a model antarctic circumpolar current." Journal of Physical Oceanography **42** (2012).

[42]P. B. Rhines and W. R. Young, "Homogenization of potential vorticity in planetary gyres," Journal of Fluid Mechanics **122**, 347–367 (1982).

[43]J. Esler, "The turbulent equilibration of an unstable baroclinic jet," Journal of Fluid Mechanics **599**, 241–268 (2008).

[44]B. Willcocks and J. Esler, "Nonlinear baroclinic equilibration in the presence of ekman friction," Journal of Physical Oceanography **42**, 225–242 (2012).

[45]J. LaCasce and K. Brink, "Geostrophic turbulence over a slope," Journal of physical oceanography **30**, 1305–1324 (2000).

[46]K. S. Smith and G. K. Vallis, "The scales and equilibration of midocean eddies: Forced-dissipative flow," Journal of Physical Oceanography **32**, 1699–1720 (2002).

[47]G. Roullet, J. C. McWilliams, X. Capet, and M. J. Molemaker, "Properties of Steady Geostrophic Turbulence with Isopycnal Outcropping," Journal of Physical Oceanography **42**, 18–38 (2012).

[48]K. S. Smith and G. K. Vallis, "The scales and equilibration of midocean eddies: Freely evolving flow," Journal of Physical Oceanography **31**, 554–571 (2001).

[49]L.-L. Fu and G. R. Flierl, "Nonlinear energy and enstrophy transfers in a realistically stratified ocean," Dynamics of Atmospheres and Oceans **4**, 219–246 (1980).